Retrieval of ground level NO_2 and O_3 by various methods and validation of satellite observations

By

Naveed Ahmad

Registration Number

00000318716

Supervisor

Professor Dr. Muhammad Fahim Khokhar

INSTITUTE OF ENVIRONMENTAL SCIENCES & ENGINEERING

SCHOOL OF CIVIL & ENVIRONMENTAL ENGINEERING

NATIONAL UNIVERSITY OF SCIENCES AND TECHNOLOGY

ISLAMABAD

2021

Certificate

It is certified that the contents of the thesis entitled **"Retrieval of ground level NO_2 and O_3 by various methods and validation of satellite observations"** submitted by **Engr. Naveed Ahmad** has been found satisfactory for partial fulfillment of requirements of the degree of Master of Science in Environmental Engineering.

Supervisor: _____
Dr. Muhammad Fahim Khokhar
Professor
IESE, SCEE, NUST

Member: _____
Dr. Muhammad Arshad
Professor
IESE, SCEE, NUST

Member: _____
Dr. Muhammad Zeeshan Ali Khan
Associate Professor
IESE, SCEE, NUST

Thesis Acceptance Certificate

Certified that final copy of MS/MPhil thesis written by **Engr. Naveed Ahmad** (Registration No. **00000318716**) of **IESE (SCEE)** has been verified by undersigned, found complete in all respects as per NUST Statutes/Regulations, is free of plagiarism, errors and mistakes and is accepted as partial fulfillment for award of MS degree. It is additionally confirmed that important changes as brought up by GEC members have likewise been incorporated in the said thesis.

Signature with stamp: _____
Name of Supervisor: _____
Date: _____

Signature of HoD with stamp: _____
Date: _____

Signature (Dean/Principal): _____
Date: _____

Declaration

I **Naveed Ahmad** certify that this research work titled "**Retrieval of ground level NO_2 and O_3 by various methods and validation of satellite observations**" is my own work. The work has not been presented elsewhere for assessment. The material that has been used from other sources it has been properly acknowledged / referred.

Naveed Ahmad

Reg. No. 00000318716

Dedication

Dedicated to my exceptional parents and adored siblings whose tremendous support and cooperation led me to this wonderful accomplishment.

Acknowledgements

I am thankful to my Creator Allah Subhana-Watala to have guided me throughout this work at every step and for every new thought which You setup in my mind to improve it. Indeed, I could have done nothing without Your priceless help and guidance. Whosoever helped me throughout the course of my thesis, whether my parents or any other individual was Your will, so indeed none be worthy of praise but You.

I am profusely thankful to my beloved parents who raised me when I was not capable of walking and continued to support me throughout in every department of my life.

I would like to express special thanks to my supervisor Professor Dr. Muhammad Fahim Khokhar for his help throughout my thesis. I would also like to thank Dr. Muhammad Zeeshan Ali Khan and Dr. Muhammad Arshad for being on my thesis guidance and evaluation committee.

I would also like to pay special thanks to members of Climate Change and Atmospheric Research Group (C-CARGO) for their tremendous support and cooperation. Each time I got stuck in something, they came up with the solution.

Finally, I would like to express my gratitude to all the individuals who have rendered valuable assistance to my study.

Copyright Statement

Table of Contents

List of Tables

List of Figures

List of Acronyms

MAX-DOAS	Multi-Axis Differential Optical Absorption Spectroscopy
AMF	Air Mass Factor
DOASIS	Differential Optical Absorption Spectroscopy Intelligent System
dSCD	Differential Slant Column Densities
NO	Nitric Oxide
NO_2	Nitrogen Dioxide
SCD	Slant Column Density
VCD	Vertical Column Density
NOx	Oxides of Nitrogen
O_3	Ozone
UV	Ultra-Violet
VOCs	Volatile Organic Compounds
WHO	World Health Organization
RMS	Root Mean Square
OMI	Ozone Monitoring Instrument
VOCs	Volatile Organic Compounds
TROPOMI	Tropospheric Monitoring Instrument
VMRs	Vertical Mixing Ratios
RMSE	Root Mean Square Error
MAE	Mean Average Error
MB	Mean Bias

Abstract

Nitrogen dioxide (NO_2) and Ozone (O_3) are criterion air pollutant and of utmost importance due to their role in atmospheric chemistry and tropospheric air pollution. Exposure to a higher level of O_3 and NO_2 has been reported to cause various health issues in humans. Ground-level measurements of tropospheric NO_2 and O_3 are valuable for studying atmospheric chemistry, atmospheric pollution, climate change and for satellite validation. In this study, ground level NO_2 and O_3 concentrations were retrieved. This study also presents the validation of vertical mixing ratios (VMRs) of Multi-Axis Differential Optical Absorption Spectroscopy (Mini MAX-DOAS) vertical column densities (VCDs) with measurements of conventional analyzers for NO_2 and O_3. The VCDs were converted to vertical mixing ratios (VMRs) in parts per billion by volume (ppbv) for validation purposes. The satellite (TROPOMI and OMI) validation was also performed by comparing the ground-based measurements with TROPOMI and OMI VMRs. Daily Mini MAX-DOAS NO_2 VMRs at an altitude of 650 m (an average BLH) and 300 m were validated with values obtained through an in situ conventional analyzer. The daily NO_2 measurements were higher during the winter season while values were lower during the summer season. The retrieved O_3 concentrations has shown highest values during the warmer months, corresponding to the observed columns of ozone. The comparison of NO_2 have shown a similar trend for VMRs of both altitudes with conventional analyzer but values at an altitude of 300 m have shown a greater agreement as less errors were detected i.e., Root Mean Square Error (RMSE), Mean Average Error (MAE) and Mean Bias (MB). The linear regression for values of both instruments has shown a strong positive correlation for NO_2 with $r = 0.73$. Similar validation was performed for O_3 measurements but found that Mini MAX-DOAS was not able to differentiate between tropospheric and stratospheric O_3 concentrations due to its sensitivity constraints for ground-level O_3. The fraction of O_3 in the stratosphere is usually higher than that in the troposphere. Therefore, the retrieval of ground-level O_3 from Mini MAX-DOAS

observations is still a challenge due to interference of the stratospheric O_3 absorption. Furthermore, the ground-based NO_2 measurements were compared with satellite observations (TROPOMI and OMI VMRs). The regression analysis showed a strong positive correlation with r = 0.72 for conventional analyzer values vs TROPOMI VMRs and r = 0.86 for MAX-DOAS VMRs vs TROPOMI VMRs. Furthermore, the Pearson correlation (r) of in situ measurements vs OMI VMRs, MAX-DOAS VMRs vs OMI VMRs and TROPOMI VMRs vs OMI VMRs was 0.54, 0.70 and 0.71 respectively.

Chapter 1

INTRODUCTION

1.1. Background

Air pollution as defined by the US EPA refers to the presence of contaminating substances in the atmosphere that interfere with human health and welfare and produce a variety of harmful environmental effects. The annual worldwide consequences of air pollution range from reduced life expectancy (of millions), damage to crops which can feed millions and increased climatic disturbances which can costs millions $. As a result of these negative consequences of air pollution i.e., climate change, increased mortality and morbidity, its position as one of this era's greatest challenges has become clear. However, because the majority of its impacts are distributed unevenly and often poorly understood, finding adequate solutions for this problem has proven to be difficult (Manisalidis et al., 2020)

Air Pollution is one of the most alarming environmental issues and is at the forefront of the critical challenges being faced by our societies. It is responsible for harmful effects on Human health as well as on the ecosystem. Moreover, air pollution is also thought to be contributing to larger-scale phenomena like the greenhouse effect and ozone layer depletion (Habeebullah, Munir, Morsy, & Mohammed, 2010).

1.2. Nitrogen Dioxide (NO_2)

Nitrogen Dioxide (NO_2), a criteria pollutant, formed as the consequence of fossil fuel consumption, includes sources like combustion processes, transportation and activities carried out in industries (Demirel, Özden, Döğeroğlu, & Gaga, 2014). Nitrogen oxides (NOx) are considered responsible for deteriorating environmental health in many ways. For example, NOx plays an active role in the destruction of the Ozone layer, NOx is a key ingredient of photochemical smog, etc. (Salonen, Salthammer, & Morawska, 2019). NO_2 concentration and impacts are increasing day by day which can be attributed to several factors like exponential

growth of population during the last few decades, more reliance on fossil fuel consumption, inefficient energy consumption, etc. Besides, there are some other natural sources of NO_2 like lightning and fire events that contribute to its emission (Frins et al., 2014). NO_x is important as it plays a key role as a primary pollutant as well as a secondary pollutant. The high temperature achieved during fossil fuel combustion results in the formation of NO and consequently NO_2 in the atmosphere makes it a primary pollutant. However, NOx reaction with ozone is viewed as its role as a secondary pollutant (Beard & Freas, 1994).

1.3. Ozone (O_3)

Ozone is one of the most important atmospheric trace gases in the stratosphere and the troposphere, affecting the earth-atmosphere radiative balance and hence the climate. 90% of the earth's ozone is concentrated in the ozone layer situated in the stratosphere, shielding the surface from the sun's harmful UV radiations. The remaining 10%, termed tropospheric ozone, is one of the criteria pollutants that reside in the troposphere and has adverse impacts on human health and vegetation. Generated mainly from anthropogenic sources, it is the 3rd largest contributor to the total tropospheric radiative forcing, with a radiative forcing of 0.40 $\pm 0.20 Wm^{-2}$, (Stocker et al., 2013). Ozone is also central to tropospheric chemistry due to its role in the initiation of photochemical oxidation processes via direct reaction, photolysis and the subsequent reactions of the photoproducts to form the hydroxyl radical (Monks, 2005). High ozone concentrations (estimated 220 ppb) were first recorded during the Los Angeles (photochemical) smog incident of 1952, characterized by low visibility, crop damage, eye irritation, objectionable odor and deterioration of rubber, (Haagen-Smit, 1952). Tropospheric ozone is termed by many as the most damaging air pollutant to vegetation, with impacts including visible leaf injury, in species composition and reduction in forest growth, (Ashmore, 2005). Research shows that O_3 pollution poses a growing threat to global food security even when reductions in future ozone precursor emissions are achieved, (Avnery et al., 2011).

Tropospheric ozone also contributes significantly to the deterioration of built infrastructure exposed to the outside air, including steel, stone, concrete, brick and wood, (Kumar and Imam, 2013). Based on its impacts, ozone was declared one of the "Criteria Pollutants" by the 1970 Clean Air Act alongside gases such as sulfur dioxide, the cause of sulfurous smog.

Being the fourth major contributor towards global warming after water vapor, CO_2 and CH_4, (Parry et al., 2007), the increase in tropospheric ozone requires immediate attention. While ozone level reductions are being achieved in most developed nations, increasing trends are being observed over most locations in Asia, including the Indian region, where the impacts of ozone are largely unknown, (David and Nair, 2013). Chronic obstructive pulmonary disease (COPD) caused due to ozone exposure causes roughly 22,000 premature deaths in 25 European Union countries, (WHO, 2012), and about 12,000 deaths in India, annually, (Ghude et al., 2016). Ozone-related deaths are estimated to make up about 5–20 % of all air pollution-related deaths at present, roughly 470,000 premature respiratory deaths globally and annually, (Silva et al., 2013). Ground-level ozone concentrations at all the major and minor urban centers must be monitored, and the impacts of various factors such as temperature and wind on its concentration and trends must be studied.

1.4. Instruments

MAX-DOAS (Multi-Axis Differential Optical Absorption Spectroscopy) is a new technique which is developed in the last few decades. It is a ground-based remote sensing technique that measures scattered light from different slant or elevation angles to obtain the differential slant column densities (dSCDs) of trace gases, present in the atmosphere. Its high sensitivity in the atmosphere (specifically lower) makes this technique more reliable than other techniques used to retrieve profiles of atmospheric gases and aerosols. (Hönninger, Friedeburg, Platt, & Physics, 2004; Pikelnaya, Hurlock, Trick, & Stutz, 2007; Platt & Stutz, 2008; Theys et al., 2007; Wagner et al., 2004; Wittrock et al., 2004).

The Chemiluminescence technique and non-dispersive ultraviolet absorption method for Nitrogen oxides and Ozone measurements have been improved since its inception. (Drummond, Volz, & Ehhalt, 1985; Fontijn, Sabadell, & Ronco, 1970; Grosjean, Harrison, & technology, 1985; Pollack, Lerner, & Ryerson, 2010; Robinson, Bollinger, & Birks, 1999). The Chemiluminescence technique uses gaseous Nitric oxide reactions with ozone in excess is used, which is added to the sample (air). The ultraviolet absorption method is based on ozone's characteristic of absorbing ultraviolet rays of a specific wavelength

1.5. Study Area

Islamabad, the capital of Pakistan is selected as a site for this study. It is located at Latitude 33.349 N; Longitude 72.324 E, with an elevation from sea level of about 540 meters (1770 ft.). Islamabad is a mountainous region located in Pothohar Plateau. Its sub-tropical humid climate has two distinct seasons: Winter (October-March) and Summer (April-September) (Parekh et al., 2001). The instrument was mounted at the rooftop of the Institute of Environmental Sciences and Engineering (IESE), NUST. The lowest elevation angle used in this study was 2° as no high structure was present in the view field of the telescope.

1.6. The Present Study

The study was formulated to achieve the following objectives:

1. To retrieve ground-level NO_2 and O_3 by MAX-DOAS and its validation with conventional methods.
2. To compare ground-level NO_2 and O_3 with satellite observations.

Chapter 2

LITERATURE REVIEW

2.1. Composition of Atmosphere

Our earth is enveloped by many gases, commonly known as air. It is divided into four layers based on the characteristics of each layer as:

2.1.1. Troposphere:

It is the lowest layer of the atmosphere and its importance originates from the weather system that exists in this layer. It is also important as most of the mass of the atmosphere exists in this layer. The thickness of the troposphere varies and is dependent on temperature and location. Its thickness ranges from 7 to 8 km at poles to 16 to 18 km as the equator. This variation is attributed to the rotation of the earth as it tends to shift air masses towards the equator. Besides temperature is always high at the equator, as compared to poles, due to unequal distribution of insolation. With the increase in height, temperature decreases in this layer (Holton et al., 1995).

2.1.2. Stratosphere

The layer above the troposphere, which extends up to 50 km, is known as the stratosphere. It is separated from the troposphere by the tropopause. It is the second major layer of the atmosphere. It is composed of 15% mass of the atmosphere and no weather exists here. It is a layer where the Ozone layer can be found which enhances the importance of this layer. The ozone layer blocks the harmful UV radiation that can cause serious problems like cancer and skin diseases. In other words, life would have been impossible to exist on this planet. In it, temperature increases with altitude. It is due to the heat which is produced as the result of ozone formation (Brasseur & Solomon, 2006; Holton et al., 1995).

2.1.3. Mesosphere

It is a layer that is present above the stratosphere and below the thermosphere and is separated by these two by stratopause and mesopause, respectively. This layer's height is up to 80 km. This layer is also important as it protects the earth from all the meteors and asteroids that enter the atmosphere by burning them (due to friction) (Roble, Experiment, & Theory, 1995). The temperature decreases with increasing altitude in this layer.

2.1.4. Thermosphere

The thermosphere is a layer that is immediately above the mesosphere and extends from 85km to 600km. It is a layer where our telecommunication satellites work and are responsible for telecommunication on earth. Here, temperature increases with altitude because this layer is largely influenced by solar activity. In it, UV radiation results in the creations of ions by photoionization of molecules (Lübken, 1999).

2.2. Air Pollution

Air pollution is mainly excess of anything in the air which alters the natural processes and affects the environment adversely. Natural and anthropogenic activities result in the release of various pollutants in the environment that not only disturb the natural cycles but also cause adverse effects on human health. Gaseous pollutants such as NO_2 (Beelen et al., 2013), Ozone (Akimoto, 2003; Brook et al., 2002; Finlayson-Pitts & Pitts, 1997), Particulate Matter (PM_{10} and $PM_{2.5}$) (Dockery & Pope, 1994; Pope III et al., 2002; Pope III, Dockery, & association, 2006; Seaton, Godden, MacNee, & Donaldson, 1995), differ in composition, chemical activities and reactions, spatial and temporal distributions, and break downtime. Exposure to such pollutants results in serious health effects. It ranges from causing cancer (Pope III et al., 2002) to respiratory disorders. In recent years studies have linked air pollution with increased mortality (Bang, Nguyen, Vu, Hien, & Assessment, 2018; Dockery et al., 1993) and reduced life

expectancy (Pope III, Ezzati, & Dockery, 2009). Persistent Organic Pollutants (POPs) are another category of air pollutants that are considered toxic due to their longer disintegration time in the environment. Their persistence is the root cause of their toxicity. POPs when entering the food chain, they start cumulating in organisms. This accumulation may cross the toxic level and cause toxicity in an organism. This process is called bioaccumulation (Schecter, Birnbaum, Ryan, & Constable, 2006).

Air pollution continues to pose a serious environmental problem in South Asia, with 30 of the 40 most polluted cities and 4 of the 5 most polluted countries located in this region (IQAir, 2019). In terms of particulate exposure, Pakistan has emerged as the second most polluted country in the world in 2019 and has suffered estimated losses of 3.8-9.2 billion dollars and 32000-76000 premature deaths as a result of air pollution in 2018 (Farrow et al., 2020; IQAir, 2019).

2.3. NO_2 (Nitrogen Dioxide): A major criteria air pollutant

Criteria pollutants are a set of pollutants that were first highlighted by the United States Environment Protection Agency for the need of regulation because of their hazardous effects on humans and the environment in the form of acid rain, smog and other health-related issues. Today, these are used to identify the quality of air. Nitrogen Dioxide (NO_2) is a pungent smell irritating gas. Its characteristic brown color is due to its ability to absorb light. It can be seen occasionally, as a brown haze, over major cities. It is a major criteria pollutant that has not been in control since the beginning. It is so because of diversity in its sources i.e., automobile emissions, power stations, factories and industries, etc. With the rapid population growth, during the last few years, an upsurge in automobiles has been observed, which is considered a major air pollution contributor worldwide (Han & Naeher, 2006). Pakistan National Environmental Quality Standard, 2010 has suggested 80 $\mu g/m^3$ of NO_2 as a limit for prevention of sensory irritation in population, for 24 hours. NO_2 exists in both, troposphere and

stratosphere. It is an important trace gas that plays a significant role in the chemistry of atmospheric in both spheres. In the stratosphere, it plays a key part in the Ozone destruction cycle and transformation of Halogen Oxides (O-X) into much less reactive species. However, in the troposphere, it is one of the significant precursors of ozone formation, Smog and acid rain. Besides, its contribution to radiative forcing also affects the chemistry of the atmosphere.

2.3.1. Sources of NO_2

Nitrogen dioxide is mostly produced due to human activities. Its higher concentrations can be found in the northern hemisphere, specifically mostly populated areas or in other words in urban centers. It is mainly due to fossil fuel burning, which provides conditions that favor the production of NOx in the environment. According to recent studies, there is high uncertainty in emission sources of NO_2 due to its shorter lifetime in the atmosphere ranging from one to few hours. However, the transport sector is considered a major emission source of NO_2 in the atmosphere. Whereas air traffic in the stratosphere results in its production in the stratosphere (Badr & Probert, 1993). Natural sources include biomass burning and agricultural practices. Moreover, emissions from the soil and microbial activities also contribute to NOx production by various processes like putrefaction affects the net NOx budget. Even thunderstorms result in the production of NOx in the environment (Ibrahim, 2009).

Methane produced from the soil when reacts with OH produces peroxy radicals (eq. 1 and 2). These radicals can oxidize nitric oxide into NO_2 (eq. 3)

$$CH_4 + OH \sim CH_3 + H_2O \qquad \text{Eq. 1}$$

$$CH_3 + O_2 + CH_3O_2 \qquad \text{Eq. 2}$$

$$CH_3O_2 + NO + NO_2 + CH_3O \qquad \text{Eq. 3}$$

2.3.2. NO_2 Chemistry in the atmosphere

In the troposphere, high temperature around 3000°C, which can be achieved in the total combustion engine and during lightning events, oxygen molecules break down into two oxygen atoms which are highly reactive in nature. These atoms react with nitrogen molecules and produce NO and NO_2, referred to as NO_x due to their Intercomparison in the atmosphere in the presence of Ozone (tropospheric). NO_2 rapidly breaks down into NO by UV radiations *(λ < 420 nm).* NO can be produced by the reaction of hydroxyl ions with methane which is released from soil. This nitrogen dioxide can also settle down on the surface in the form of HNO_3 or acid rain (Guenther et al., 2000). Microbial activity in soil produces N_2O which is comparatively stable. This N_2O when diffuse into the stratosphere, it became unstable due to presence of shorter wavelength radiation (λ =*185- 230 nm*) and breaks down into N_2 and O atom. This oxygen atom then again reacts with N_2 to form NO which converts into NO_2 in the presence of O_3. The tropospheric NOx cycle in the atmosphere is shown in Fig. 1.

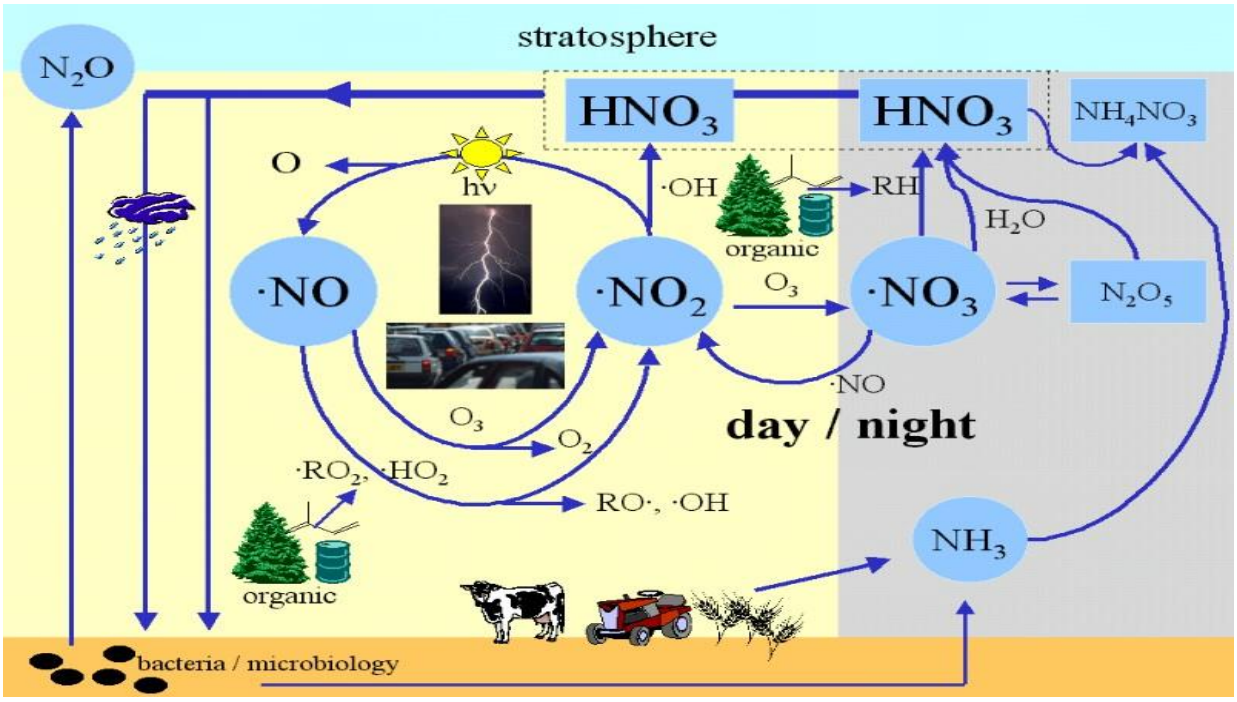

Figure 1:*The tropospheric NOx cycle in the atmosphere*

During the daytime, the interconversion of NO and NO_2 results in a Null cycle in which net production of the reaction is zero. Nitric oxide reacts with an ozone molecule to produce

nitrogen dioxide and oxygen molecules (eq.4) (Kreher et al., 2019).

$$NO + O_3 \rightarrow NO_2 + O_2 \qquad \text{Eq. 4}$$

Produced nitrogen dioxide breaks down in the presence of UV ($\lambda < 420$ nm) into nitric oxide and an oxygen atom (eq.5).

$$NO_2 + UV\ (\lambda < 420\ nm) \rightarrow NO + O\ (3P) \qquad \text{Eq. 5}$$

This oxygen atom reacts with an oxygen molecule to form ozone again (eq. 6).

$$O\ (3P) + O_2 \rightarrow O_3 \qquad \text{Eq. 6}$$

However, this cycle breaks down in the absence of UV radiations where nitrogen dioxide reacts with oxygen atom instead and produces oxygen molecule along with nitric oxide, and breaks null cycle (eq. 7).

$$NO_2 + O\ (3P) \rightarrow O_2 + NO \qquad \text{Eq. 7}$$

2.3.3. Impacts of NO_2

Nitrogen Oxides affect life, both aquatic and terrestrial. When Nitric oxide gets to mix with ozone, it initiates the catalytic conversion of nitrogen dioxide into nitric oxide. This cycle continues naturally and maintains a balance. Due to anthropogenic activities, this cycle gets disturbed. Due to the vehicular emissions and burning of fossil fuels in large quantities, habitat is adversely affected. Conditions turn worse when NO_2 is converted into nitric acid and settles down in the form of acid rain (Seangkiatiyuth, Surapipith, Tantrakarnapa, & Lothongkum, 2011). However, when NO_2 accumulates in urban areas, in certain meteorological conditions, pollution episodes are likely to happen like that of smog which not only affects the lungs, eyes and skin if exposed to humans but also affects the economic activities of the affected area.

NO and NO_2 are toxic in nature. These gases are mainly inhaled by humans from sources like industrial work and traffic. When NO_2 enters the body, it starts accumulation and turns into Nitric acid which affects the iron present in our blood thus denaturing the functionality of hemoglobin in our body. Due to the low solubility of NO_2 in water, it can travel or reach deep into our lungs and can damage our lungs. Short-term exposure can irritate breathing but ling term exposure can result in loss of functioning of lungs tissue in extreme cases (Pandey, Kumar, & Devotta, 2005).

2.4. Ground-level Ozone (O_3): A major criteria air pollutant

Ozone is one of the most important atmospheric trace gases in the stratosphere and the troposphere, affecting the earth-atmosphere radiative balance and hence the climate. 90% of the earth's ozone is concentrated in the ozone layer situated in the stratosphere, shielding the surface from the sun's harmful UV radiations. The remaining 10%, termed tropospheric ozone, is one of the criteria pollutants that reside in the troposphere and has adverse impacts on human health and vegetation. Generated mainly from anthropogenic sources, it is the 3rd largest contributor to the total tropospheric radiative forcing, with a radiative forcing of 0.40 ±0.20Wm−2 (Stocker et al., 2013). Figure 2 depicts the production of ground-level ozone through the reactions between precursor pollutants in the presence of sunlight.

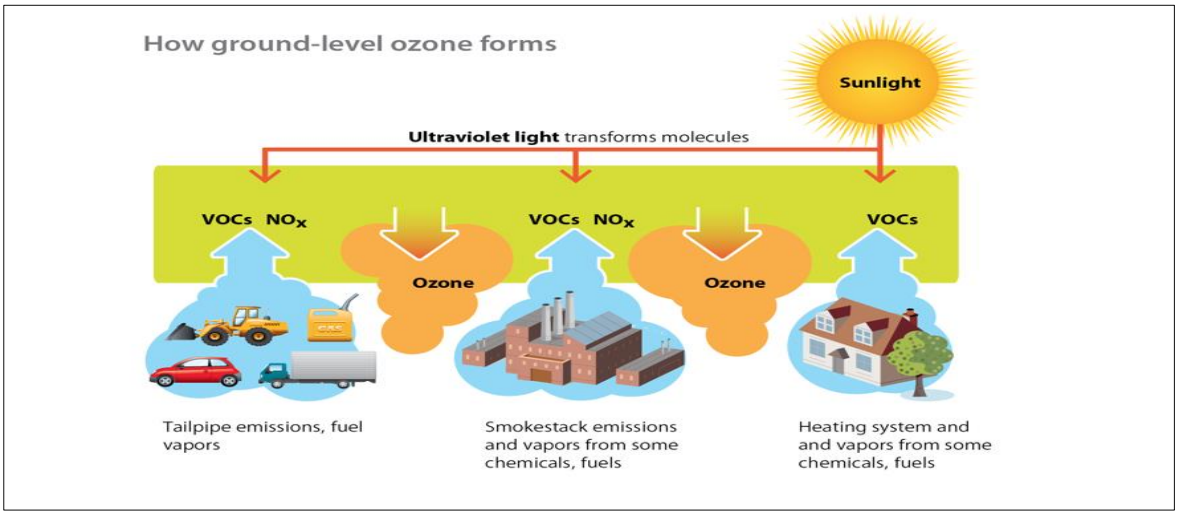

Figure 2:*Formation of ground-level ozone*

Ozone has a very short global mean lifetime in the troposphere (~3 weeks) compared to other long-lived species, with sources and sinks that vary greatly across temporal and spatial scales, (Lelieveld et al., 2009). Due to its shorter lifetime and varied sources, it is also not mixed well, resulting in large spatial and temporal variations over seasonal, annual and decadal timescales. These varied trends are further reinforced by its strong dependence on sunlight and precursor emissions, which have both natural and anthropogenic sources that can vary greatly across time and space, (Cooper et al., 2014). Understanding tropospheric ozone chemistry is essential as it is a powerful greenhouse gas and a precursor for the highly reactive hydroxyl radical, which determines the chemical composition of the troposphere, (Finnan et al., 1997).

2.4.1. Sources of ground-level O_3

Photo-oxidation of CH_4, CO, Non-methane hydrocarbons (NMHCs) and volatile organic compounds (VOCs) in the presence of a sufficient amount of NO_x in the air and sunlight result in the production of ozone. NOx is the limiting factor in the production of tropospheric ozone, controlling its production and destruction, (Lin et al., 1988). The major portion of precursor emissions are generated from anthropogenic sources such as vehicular emissions and industrial emissions, (Cooper et al., 2014), however natural emissions of precursor compounds also play a significant role in regulating ozone concentrations, especially in rural areas where anthropogenic sources are largely absent. Some natural sources of ozone precursors include soil NO_x emissions, lightning NO_x emissions, biogenic VOC (BVOC) emissions, wildfire emissions and wetland methane emissions, (Lu et al., 2019b).

Microbial activity in soil accounts for 10-15% of all global NO_x emissions, (Hudman et al., 2012). It is dependent on the availability of inorganic nitrogen, type of vegetation and climatic conditions such as temperature and moisture, (Vinken et al., 2014). A study of European forests found soil temperature and moisture to be responsible for 74% of the observed variations in soil NO_x emissions, (Schindlbacher et al., 2004). Soil NO_x emissions increase exponentially

with soil temperature until 30°C, above which water becomes the limiting factor. High soil moisture reduces oxygen in the soil, increasing de-nitrification and reducing NO_x production, (Yan et al., 2005).

Daily NO_2 observations made by OMI satellite during the summer monsoon season in three remote rural locations in India recorded rapid and intense bursts of NO_x emissions, caused by sudden shifts from dry to wet conditions, (Ghude et al., 2010). Bursts of NO_x emissions were also observed over a 2 million hectare agricultural region in Montana through SCIAMACHY observations in the USA, following fertilizer application and subsequent precipitation, (Bertram et al., 2005).

The energy produced by lightning flashes dissociates and converts atmospheric N_2 molecules into NO_x, accounting for an estimated 2 to 8 Tg N/yr, (Murray et al., 2012). Lightning NO_x emissions make a significant contribution (10ppbv) to the upper tropospheric ozone, (Hudman et al., 2007) where ozone production is most efficient, and ozone has a longer lifetime, (Banerjee et al., 2014). Model projections over 169 Chinese cities in 2016 and 2017 (the 2 years with highest surface ozone) were made using the GEOS-Chem chemical transport model to discover contributions of anthropogenic, background and individual natural sources to surface ozone. Large contributions from natural sources (80% in March-April and 72% in May-August) were discovered, among them, lightning NOx emissions and ozone transport from the stratosphere both lead to ozone enhancements of over 20 ppbv in western China during March-April. Biogenic volatile organic compound (BVOC) emissions were discovered to enhance MDA8 ozone by more than 15 ppbv in eastern China during July-August, (Lu et al., 2019a).

Biogenic VOCs are important ozone precursors, generated during photosynthesis and vary greatly across plant species. Field and laboratory observations show an exponential rise in biogenic isoprene and monoterpene emissions with rising temperature, (Guenther et al., 2006), determining temperature as the limiting factor. The exponential rise of BVOC emissions with

temperature also drives the positive ozone-temperature correlation found over urban areas where NO_x levels are high, (Lu et al., 2019a). Wildfires release large amounts of ozone precursor gases (CO, NO_x and VOCs) and produce roughly 3.5% of the total ozone produced annually, (Jaffe and Wigder, 2012). Combustion efficiency plays a significant role in determining the secondary emissions from a wildfire event. Flaming combustions resulting from high temperatures support high combustion efficiency, causing stronger oxidation of fuel nitrogen compounds, leading to higher NO_x emissions and ultimately higher ozone production. Whereas smoldering combustions resulting from cooler conditions release higher levels of reduced nitrogen compounds such as NH_3 which are not favorable for ozone production, (Jaffe and Wigder, 2012). Smoldering wildfires however cause ozone enhancement downwind as the low temperatures convert NO_x to PAN which can travel significant distances away from the burning sites, (Alvarado et al., 2010)

2.4.2. Chemistry of O_3

Chemistry of Ozone depends upon various factors:

2.4.2.1. Clouds:

Clouds strongly impact the photochemical processes in the lower half of the troposphere. Water vapor saturation in the air prevents penetration of reaction-initiating sunlight. Aqueous-phase processes reduce the gas-phase concentration of precursor chemicals and produce ozone-depleting compounds, (Jonson and Isaksen, 1993). Formaldehyde (CH_2O) is a major intermediate gas in the oxidation of various hydrocarbons (e.g., ethene, isoprene, and methane) released by forests, biomass burning, traffic and industrial processes. CH_2O breaks down at an accelerated rate in the aqueous phase, creating oxidation products that react with ozone, acting as a significant sink. Furthermore, cloud processing of nitrates depletes NO_2, the limiting factor for the production of tropospheric ozone, (Lelieveld and Crutzen, 1991).

2.4.2.2. Seasons:

The onset of summer monsoon causes a decline in tropospheric ozone over southeast Asia from May to August, observed through satellite and ground observations, (Safieddine et al., 2015). Cleaner marine air input and stronger air uplift during the wet monsoon, (Sahu et al., 2014) and the cloudy, cool and wet weather conditions cause a drop in ozone chemical production, (Ojha et al., 2012). Quantification of constituent processes across the Indian lower troposphere from May to August showed a 4.2 Tg decrease in chemical ozone production and uplifting of 3.3 Tg ozone (due to strong convection); leading to significant decreases in the Indian lower tropospheric ozone during the monsoon months, (Lu et al., 2018). The uplifted ozone is transported by the easterly jet in the upper troposphere to the rest of the globe, impacting global tropospheric ozone distribution, (Lelieveld et al., 2018). Differences in the strength of the monsoon system can cause variations of as much as 3.4 ppbv, (Lu et al., 2018). A similar negative correlation between ozone levels and monsoon strengths has been found at Pacific Ocean sites near the Asian continent, (Hou et al., 2015). The outflow of ozone to the East China Sea during stronger East Asian summer monsoons has been shown to increase surface ozone concentrations over central and western China, (Yang et al., 2014).

2.4.2.3. Temperature:

A 3°K rise in temperature increases biogenic isoprene emissions by 6-31%, in turn increasing surface ozone by more than 2 ppbv in northern mid-latitudes, (Doherty et al., 2013). The enhanced isoprene levels also lead to the production of more peroxyacetyl nitrate, PAN (a NO_x reservoir compound), which can travel long distances and produce ozone downwind, (Fiore et al., 2012). Models project a significant rise in BVOC emissions as the result of global warming, resulting in higher tropospheric ozone concentrations, (Unger et al., 2006). Rising temperatures and dry weather conditions due to global warming have been conclusively linked with an increase in intensity and frequency of wildfires in the western US since 1970, (Westerling et al., 2006). Large wildfire events occur more frequently with a rise in temperature and solar

radiation, and with decreasing humidity and wind speed, with four times as many large wildfire events as small wildfire events at temperatures above 30°C, (Lu et al., 2016).

2.4.2.4. Meteorology:

Meteorology impacts tropospheric ozone production by regulating the efficiency of deposition of various precursor and intermediate substances such as PAN (Peroxyacetyl Nitrate), HO_x (water vapor) and dry deposition of tropospheric ozone, (Lu et al., 2019b). PAN is generated through the oxidation of acetaldehyde in the hydrocarbon-rich environment using NO_x as a catalyst, (Brasseur and Jacob, 2017). The formation process of PAN serves as a sink for both NO_x and peroxy radicals, reducing ozone production in and around the region. It acts as a NO_x reservoir compound, traveling across the colder higher troposphere, transporting NO_x from highly polluted regions and fire spots to remote regions where it reacts with other precursors in the presence of sunlight to produce ozone, (Alvarado et al., 2010) (Fischer et al., 2014). Rising global temperatures are projected to cause rapid PAN decomposition, increasing ozone production in polluted regions and reducing it in remote regions as transport of PAN (through colder higher troposphere) will no longer be dominant, (Doherty et al., 2013)

Atmospheric water vapor content is essential to ozone photochemistry especially in remote areas where NO_x levels are low and ozone removal by HO_x is effective, generating significant negative correlations between ozone column densities and relative humidity, (Lu et al., 2016). In polluted regions where NO_x levels are relatively high, water vapor has competing effects on ozone production. Hydroxyl radical (OH) oxidizes CO and hydrocarbons and activates ozone production, while simultaneously terminating ozone formation by converting NO_2 to nitric acid (HNO_3), (Banerjee et al., 2016). Globally, the increasing temperature would lead to more evaporation and evapotranspiration, increasing the water vapor content of the air and leading to a decline in tropospheric ozone burden, (Von Schneidemesser et al., 2015).

2.4.2.5. Deposition:

Dry deposition on vegetation acts as a sink for 20% of total annual tropospheric ozone, (Fowler et al., 2008). Dry deposition occurs mostly through stomatal uptake on leaf surfaces and is dependent on climatic factors such as light, temperature, soil moisture and humidity, (Hardacre et al., 2015). Adverse weather conditions such as drought and high air or soil temperatures suppress stomatal uptake to protect against desiccation, increasing ozone levels in semi-arid regions as well as high latitude regions on hot dry days, (Anav et al., 2018). The remaining portion of dry deposition is attributed to non-stomatal ozone deposition i.e. the thermal decomposition of ozone with external surfaces including soil and canopy; and is also dependent on temperature and solar radiation, (Monks et al., 2015). Projections of future surface ozone over Europe using chemistry transport models (CTMs) have predicted increased ozone dry deposition during winter due to reduced snow cover, whereas in summer, changes in soil moisture, temperature and air stability will suppress ozone dry deposition, leading to a 6 ppbv rise in ozone over Europe. The relatively weaker process of dry deposition accounts for more than 60% of the total ozone enhancements, making it a key player in climate-induced future ozone changes, (Andersson and Engardt, 2010).

Due to lifetimes reaching several weeks up to months, ozone and its precursor's compounds travel across large distances from polluted regions to pristine areas where little to no anthropogenic emissions are present, (Young et al., 2013).

2.4.3. Impacts of ground-level O_3

Ozone is a very strong oxidizing agent, contributing enormously to the oxidative capacity of the atmosphere (Monks, 2005). Ozone plays a major role in atmospheric chemistry by dominating the formation of hydroxyl radical, which in turn impacts the lifetimes of various trace gases such as methane and hydro-chlorofluorocarbons (HCFC) (Finlayson-Pitts and Pitts, 1993). The biological effect of ozone is attributed to its stability to cause oxidation of biomolecules, directly as well as through various free radical reactions (Mustafa, 1990). It is

the major constituent of photochemical smog and causes various health impacts in plants and humans, resulting in its status as one of the criteria air pollutants.

The oxidative potential of ozone initiates various reactions in the human body, including lipid peroxidation and loss of functional groups of enzymes, alteration of membrane permeability, and cell injury or death. The most pervasive impacts are in the form of various lung injuries. Injury to ciliated cells in the airways and the type 1 epithelial cells in the alveolar region have been attributed to acute exposure to O_3. The most evident proof of damage is seen as a loss of cells and accumulation of inflammatory cells at the junction of terminal bronchioles and alveolar ducts. The human body rebounds from short-term exposure through the initiation of a recovery phase, where cell damage and loss of enzyme activity during exposure is followed by increased metabolic activities, coinciding with a proliferation of metabolically active cells. Chronic exposure to ozone on the other hand can exacerbate lung diseases and increase the chances of lung tumors in susceptible populations. Besides the impacts on the lungs, ozone exposure also causes extra-pulmonary effects involving the blood, spleen, central nervous system, and other organs. O_3 may also act in synergy with other air pollutants in photochemical smog such as NO_2 to produce enhanced effects. The major pathway of resistance against ozone poisoning is an increase in uptake of dietary antioxidants such as vitamin E, vitamin C, and selenium (Mustafa, 1990).

Tropospheric O_3 is highly phytotoxic, causing both acute (symptomatic) and chronic (changes in growth, yield or productivity and quality) impacts, the latter being an increasingly prevalent problem in both crops and forests (Krupa and Manning, 1988). Tropospheric ozone reduces vegetative productivity (Ainsworth et al., 2012). As the precursors of ozone, NO_2 and VOCs are also generated from natural sources such as lightning and specialized vegetation. The problem of ozone is not limited to cities or polluted places. Ozone has been recognized as the most important rural air pollutant, affecting human health as well as the vegetation of all kinds

(Ashmore, 2005).

The concentration of O_3 in the air and stomatal conductance determine the rate of O_3 uptake. When stomata are open, O_3 can gain access to the interior of leaves, where it reacts with lipid and protein components of cell walls and plasma membranes, leading to the formation of aldehydes, peroxides and assorted reactive oxygen species. These products can then activate various transduction pathways for defense responses: stomatal closure, production of antioxidants such as ascorbate, phenolics and isoprenoids; and programmed cell death (Lindroth, 2010).

2.5. Measurement Techniques

Since 19th Century, innovations have improved the instrumentation and methods being used to monitor ambient air quality. Today we have an instrument with approximately 99% precision and accuracy. Several techniques are there that are being used to measure trace gas concentrations in ambient air. The applied techniques being used are as follows:

2.5.1. Chemiluminescence Methods

The Chemiluminescence technique for Nitrogen oxides measurement has been improved since its inception in 1970-80s (Drummond, Volz, & Ehhalt, 1985; Fontijn, Sabadell, & Ronco, 1970; Grosjean, Harrison, & technology, 1985; Pollack, Lerner, & Ryerson, 2010; Robinson, Bollinger, & Birks, 1999). Gaseous Nitric oxide reactions with ozone in excess is used, which is added to the sample (air). Light of a specific wavelength is emitted from excited NO_2 production. The intensity of emission is measured either solid-state detector or by photomultiplier tubes (PMT), and it is directly proportional to the NO concentration in the sample used. Nitrogen Dioxide measurement requires its regulated reduction to Nitric oxide either by photolytic conversion or by thermal decomposition, where NO_2 is derived by a differential method.

2.5.2. Colorimetric Methods

In this method, colored species are produced when NO_2 is allowed to react with organic dye solutions. According to Beer Lambert's Law, optical absorbance of a chemical species is directly proportional to the amount of that species absorbed in solution or in other words, the concentration of that species which is then measured by spectrophotometer. It is a sensitive method as it is measured by spectrophotometer and dyes are needed to be analyzed immediately after the reaction as color complex forms in this process are quite unstable. One major limitation of this method is the unavailability of facilities in the field and remote areas. Many analyzers have been designed on this principle (Chen et al., 2016; Riess & Standards, 1998) for NO_2 monitoring by the USEPA, Occupational Safety & Health Administration (OSHA) and National Institute for Occupational Safety and Health (NIOSH).

2.5.3. Electrochemical Sensor

Electrochemical sensors are cost-effective and portable sensors that are being used to measure ambient air quality. High sensitivity, cheaper price and longer sample retention time make these sensors better among all other samplers. Its working principle is based on the electrochemical reduction of gasses between electrodes, dipped in an electrolyte.

2.5.4. Passive Samplers

For several years, the passive sampling method is being used for monitoring air pollutants. In this technique, Plastic bags and membranes are deployed and employed at the site. By the process of diffusion, gas is diffused in a precise amount in the passive sampler which is calculated through its partitioning co-efficient relative to the sampler.

2.5.5. Satellite Remote Sensing

Satellite observation has been considered and acknowledged widely as an important tool for the quantitative evaluation of the distribution of atmospheric gases and composition (Beirle, Platt, Wenig, Wagner, & Physics, 2003; Burrows, Platt, & Borrell, 2011; Fioletov et al., 2013;

Lee et al., 2011; Lin, McElroy, & Physics, 2011; Martin, 2008; Richter, Burrows, Nüß, Granier, & Niemeier, 2005; Van Der A et al., 2008). In the past few years, a lot of work has been done to study the emissions, sources, variation characteristics in different regions of the world, with satellite data e.g., for SO_2 (Boynard et al., 2014; Fioletov et al., 2013; C. Li et al., 2010), aerosols and NO_2 (Hilboll, Richter, Burrows, & Physics, 2013; Richter et al., 2005; Van Der A et al., 2006; S. Wang et al., 2012).

2.5.6. Spectroscopic Method (DOAS)

Differential Optical Absorption Spectroscopy (DOAS) is a reliable, sensitive and common technique to monitor atmospheric composition. It was first used by Plat and his coworkers in 1979. Its measurement of atmospheric trace gases is done by the light source. In past, it has been applied to calculate the concentrations of many trace gases including, Hypobromite (BrO) by Sanders *et al.*, 1988 in the stratosphere and by Hausmann and Platt, 1994 in the troposphere, Nitrous acid (HONO) by Perner and Platt in1979 where by Platt in 1980, Formaldehyde (CHOCHO) by Volkamer *et al.* in 2005 and Nitrate (NO_3) by platt et al. in 1980. Besides, many other trace gases absorb Ultra-Violet and Visible region that can be measured through this technique (PlattU, 2008), such as O_3, NO_2, SO_2, HCHO, OClO, H_2O and NH_3. It can measure several trace gases concurrently, which not only saves time but also allows analysis of different components of observed air masses. Generally, DOAS is performed using an artificial light source, known as the active DOAS technique, and can be performed passively with natural light sources i.e., extraterrestrial light sources.

Chapter 3

INSTRUMENTATION AND METHODOLOGY

3.1. Mini Max-DOAS Instrument:

To quantify the tropospheric trace gases, the MAX-DOAS uses different elevation angles, from 0 to 90°, to capture the scattered sunlight (Bobrowski, Hönninger, Galle, & Platt, 2003). MAX-DOAS can measure many trace gases, at a time, in a visible and Ultra-Violet Spectral range and resultant less residual allows its use in even less polluted environment. It is a light weighted instrument with dimensions of 13cm×19cm×14cm. MAX-DOAS instrument used in this study contains a 40mm lens mounted at the front, coupled with spectrograph by fiber optics and electronic circuit. Czerny-Turner spectrometer (USB 2000+, Ocean Optics In.), having a spectral resolution of 0.7 nm records the scattered light of absorption spectra between 320-460 nm. The stepper motor, installed in it, is used to move the entire instrument to achieve desired elevation angle. Scattered light enters the instrument via a lens that is tightly sealed to avoid any condensation of water vapors and prevent dust particles to damage the interior optics. The instrument is shown in Fig. 3.

Figure 3:*Mini MAX-DOAS instrument*

3.1.1. Working Principle:

Lambert-Beer law is the working principle of the DOAS technique, which states that transmittance of light i.e., electromagnetic radiation, is directly proportional to the concentration of a substance present in the optical path. It is presented in Eq. (8)

$$I(\lambda)=Io\ (\lambda)\ e - \alpha LC \qquad \text{Eq. 8}$$

Here, "Io" means incident intensity whereas "I" is referred to as measured intensities. This technique depends upon the difference in wavelengths is observed and the reference spectrum. Various trace gases can be obtained simultaneously within a selected fitting interval. It considers specific cross sections and by using spectra of desired gases, differential slant column densities (dSCDs) can be retrieved. DOAS technique is used for the retrieval of trace gases in the atmosphere.

Differential Optical Absorption Spectroscopy Intelligent System (DOASIS) is used to run the Mini MAX-DOAS instrument for the acquisition of the spectra. It also performs other important functions like controlling the stepper motor, Setting Peltier temperature, adjusting integration time of each spectrum, etc. A JavaScript is used to run the DOASIS which includes all the commands for its functioning. It can also be used for the calculation of the ring spectrum, which is required for the analysis in QDOAS. Dark current and Offset can be measured from this software manually.

A dark current is a small current that is monitored for photosensitive devices like spectrometer. For its measurement, large Tini (Exposure/integration time) and fewer scans are selected. Offset is the measurements recorded in the "No photons" condition, in other words, it is measured in dark conditions. However, a smaller integration time and high scans are used for measuring offset spectra as shown in Table 1.

Table 1:*Values usually used for Dark Current and Offset measurement*

Parameter	Integration/Exposure time(milliseconds)	Scan numbers
Dark Current	10000	01
Offset	100	1000

3.2. Windows Differential Optical Absorption Spectroscopy (WinDOAS):

3.2.1. Wavelength Calibration:

For wavelength calibration, WinDOAS (Windows Differential optical absorption spectroscopy) was used. A spectrum taken at noon was used for the calibration purpose (usually taken at 90^{o} of noontime/with least SZA). In calibration, the fit was applied between a measured and a convoluted spectrum. Meanwhile, the wavelength of the solar spectrum was attributed to the individual detector's pixels (2048). The calibration fit is also known as "Kurucz-fit" because a solar spectrum measured by Kurucz is usually used as input which is further convoluted as per the spatial resolution of the mini MAX-DOAS used in the monitoring. The wavelength range was divided into several sub-windows (sub windows= 6) for analyzing the fits in each sub-window. For adjustment of spectrum shift between convoluted and measured spectra, "shift and squeeze" was also applied. Slit Function Parameter (SFP) specifies that the interpolation of the results of the individual sub-window was carried out using polynomial degree. Repeated twice the calibration process, reduces the residual. All measure spectra are evaluated in this study using the calibration file against a reference spectrum.

3.2.2. Wavelength Convolution:

This process was performed by using the "Convolution tool" of WinDOAS software. It is a mathematical process that is important for wavelength processing operations.

3.3. NO_2 analysis:

This is performed in QDOAS software. The selected NO_2 analysis window was 409 nm to 445 nm. The wavelength range was chosen because of the lowest possible residual errors and DOAS fit result. For analysis, calibrated spectrum was used as a reference spectrum. Different cross-sections: NO_2 at 298 K (Vandaele et al., 1996), NO_2a at 220 K (Vandaele et al., 1996), O_3 at 223 K (Serdyuchenko, Gorshelev, Weber, Chehade, & Burrows, 2014), O_4 at 293 K (Thalman & Volkamer, 2013), H_2O (Rothman & Transfer, 2010) and Ring were used. A polynomial of 4th degree was used for NO_2 analysis. Some fields/parameters in the "Output Tab" were selected which is required in the results i.e., Solar Zenith Angle (SZA), RMS (root mean square/residue), Elevation viewing angle and integration time, etc. Then finally, the output file path was given where the files wanted to be stored the analysis was performed on all measured spectra and NO_2 dSCDs and results were obtained in an ASCII file. NO_2 Analysis window in QDOAS, showing fitting interval used for Nitrogen dioxide is presented in Fig. 4

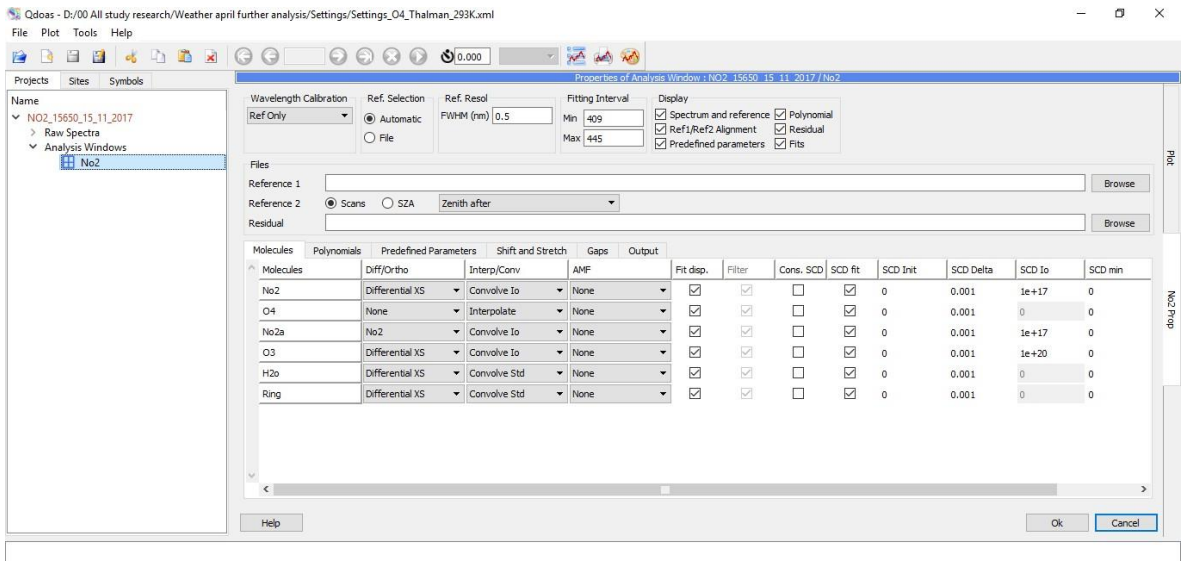

Figure 4:*NO_2 Analysis window in QDOAS, showing fitting interval used for Nitrogen Dioxide*

3.4. O_3 Analysis:

The cross-sections of different trace gases used in the convolution process with their convolution specifications and analysis windows for O_3 analysis are listed in Table 2. "Standard convolution" (Convolve Std) tool is used to convolute the cross-sections with the highest resolution. Slit function type

Gaussian (FWHM = 0.7 nm) and standard calibration are used. The "I_0 correction" (Convolve I_0) tool is used to evaluate the optical depth in convolution (Schreier et al., 2015). Analysis window in QDOAS showing fitting interval used for Ozone is presented in Fig. 5.

Table 2:*Cross-sections of different trace gases with their convolution specifications*

Parameter	O_3 settings for DOAS fit
Fitting window	320-341nm
TO_3	TO_3_223K_SDY
TO_3A	TO_3A_293K_SDY
PO_3B	PO_3B_SDY_Pukite1
PO_3D	PO_3D_SDY_Pukite2
O_4	O_4_Hermans
HCHO	HCHO_297K_Meller
NO_2	NO_2_298K_VanDaele
BrO	BrO_223K_Fleischmann
Polynomial Order	4th polynomial order: Calibration based on Fraunhofer lines of Kurucz solar spectrum (Kurucz, 1984)
Ring	Ring (4th polynomial order was used for spectral fitting, calculated based on Kurucz solar atlas)
Intensity Offset	No

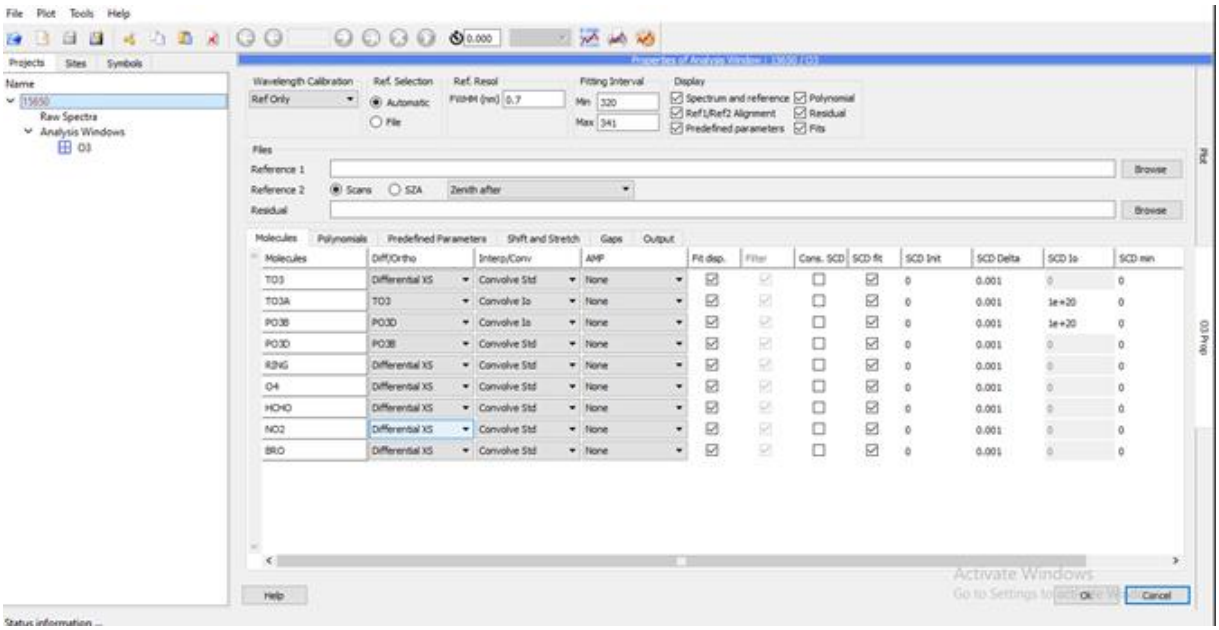

Figure 5:*O_3 Analysis window in QDOAS, showing fitting interval used for Ozone*

3.5. Air Mass Factor and VCD Calculation using MS Excel:

Microsoft Excel was used in this study to calculate VCDs by using geometric air mass factor application. AMF is a ratio of actual path distance of solar radiations and vertical path. AMF calculations are used to convert the SCDs (Slant column densities) into VCDs (Vertical column densities). Air mass factor (AMF) is usually calculated using the radiative transfer model but in this study, AMF was estimated using the geometric approximation method (Hönninger et al., 2004; Wagner, Ibrahim, Shaiganfar, & Platt, 2010; Wittrock et al., 2004). This method allows the retrieval of column densities of trace gases even in cloudy conditions (Wagner et al., 2010).

$$VCD = SCD/AMF \quad \text{Eq. 9}$$

Here differential air mass factor (dAMF) is used because the slant column densities obtained were differential SCDs (Liu et al., 2016):

$$VCD_{trop} = dSCD\alpha \,/dAMF\alpha \quad \text{Eq. 10}$$

dAMF is a difference in AMF obtained at a certain angle and AMF obtained at 90^o:

$$dAMF\alpha = AMF\alpha - AMF90° \quad \text{Eq. 11}$$

So, eq (10) will be:

$$VCD_{trop} = dSCD\alpha \,/AMF\alpha - AMF90° \quad \text{Eq. 12}$$

Using geometric approximation, AMF can be found as:

$$AMF = 1/\sin\alpha \quad \text{Eq. 13}$$

Then Eq. (12) will be:

$$VCD_{trop} = dSCD\alpha \,/\, 1/\sin(\alpha - 1) \quad \text{Eq. 14}$$

3.6. Conventional Analyzer's

3.6.1. NOx analyzer:

APNA-370 was used in this study for in situ NO_2 measurements. It uses the chemiluminescence technique as its working principle. This instrument continuously monitored the concentrations of NO_2 in the atmosphere. When ozone is added to the sample gas having nitrogen oxide, a part of nitrogen monoxide in the sample is oxidized to nitrogen dioxide and some of the generated NO_2 is excited (NO_2*), which emits light in the de-excitation state. This light emission phenomena is called chemiluminescence.

$$NO + O_3 \rightarrow NO_2^* + O_2 \qquad \text{Eq.15}$$

$$NO_2^* + NO_2 + hv \qquad \text{Eq.16}$$

This reaction is very fast and involves only NO, affected little by the various other coexistent gases. When the NO amount is low, the light intensity is in proportion to its concentration. The method using this reaction to monitor NO concentration is called chemiluminescence method. In APNA-370, the sampled gas is divided into two flow streams: one is used for NOx (NO + NO_2) measurement by reducing NO_2 to NO with a NOx converter; the second is used for NO n measurement directly. These sample gases are switched to the NOx, NO, and reference gas lines each 0.5 s with valves (solenoid), and are sent to the reaction chamber in turn. While, the open air is separately sucked by the air filter that is dried by a self-reproducing type silica gel dryer, and used to generate ozone in an ozonizer. Then, the produced ozone is sent to the reaction chamber. In the reaction chamber, the sample and ozone react, and the light emission observed in the reaction is detected by the photodiode. This instrument measures NO, NO_2, NOx concentrations from the outputs obtained by the photodiode, which are proportional to the NOx and NO values, and outputs the results as continuous signals. The instrument is shown in Fig. 6.

Figure 6:*NOx analyzer*

3.6.2. Ozone (O_3) analyzer:

The APOA-370 is an ambient ozone (O_3) monitor. This instrument uses the non-dispersive ultraviolet absorption (NDUV) method as its operating principle. This monitor continuously monitored the values of O_3 in the atmosphere for the study period. The ultraviolet absorption method is based on ozone's characteristic of absorbing ultraviolet rays of a specific wavelength. In this method, the sample gas which has passed through the filter is divided into two flow paths. The sample gas in one path is introduced to the deozonizer, where its ozone is eliminated, and then sent to the cell as "reference gas." The sample gas in the second path is sent to the cell directly, as "sample gas," by switching a solenoid valve. The measurement cell is exposed to direct radiation by a low-pressure mercury lamp which produces ultraviolet rays with a central wavelength of 253.7 nm, and a detector, which involving a photodiode and electric system to obtain electric signals, measures ultraviolet absorption by ozone. The "sample gas" and the "reference gas" are sent to the cell alternately, switched by 1 Hz with the solenoid valve. The difference in ozone content between the reference gas and the sample gas can be obtained from the difference in the measured ultraviolet absorption. The instrument is shown in Fig. 7.

Figure 7:*O_3 analyzer*

3.7. Calculation of Vertical Mixing Ratios:

Vertical mixing ratios were calculated from VCDs of NO_2 and O_3. VCDs obtained in molec/cm^2 were converted to molec/cm^3 at a specific altitude by using Eq. (17).

$$VCD_h = VCD/100 \times h \quad \text{Eq. 17}$$

Where VCD_h are VCDs at a specific altitude and h is the height/altitude in atmosphere. Then air density (ρ_{air}) was calculated through Eq. (18)

$$\rho_{air} = (P_h/M_a) \times n \quad \text{Eq. 18}$$

Where P_h is atmospheric pressure at specific height, M is molecular weight of air and n is number of moles. Then air density was converted to molec/cm^3 by using Eq. (19)

$$\rho_{air1} = \rho_{air} /10^6 \quad \text{Eq. 19}$$

The specific gas to air ratio/VMR was found using Eq. (20)

$$VMR = VCD_h / \rho_{air1} \quad \text{Eq. 20}$$

Finally, the VMRs in ppbv for a particular gas was calculated by Eq. (21)

$$VMRs = VMR \times 10^9 \quad \text{Eq. 21}$$

The overall calculation is shown in Fig. 8.

	Date	NO2 VCD (molec/cm2)	NO2_molec/cm3	pressure air_300m	airdensity_molec/m3	air_molec/cm3	NO2_air_ratio	MAX-DOAS NO2 VMRs (ppb)
2	2021-02-03	1.02338E+16	1.57E+11	940.84	1.95573E+25	1.95573E+19	8.05E-09	8.05
3	2021-03-03	1.65362E+16	2.54E+11	940.84	1.95573E+25	1.95573E+19	1.30E-08	13.01
4	2021-04-03	1.65433E+16	2.55E+11	940.84	1.95573E+25	1.95573E+19	1.30E-08	13.01
5	2021-05-03	1.04938E+16	1.61E+11	940.84	1.95573E+25	1.95573E+19	8.25E-09	8.25
6	2021-07-03	9.26074E+15	1.42E+11	940.84	1.95573E+25	1.95573E+19	7.28E-09	7.28
7	2021-08-03	8.87298E+15	1.37E+11	940.84	1.95573E+25	1.95573E+19	6.98E-09	6.98
8	2021-09-03	1.66218E+16	2.56E+11	940.84	1.95573E+25	1.95573E+19	1.31E-08	13.08
9	2021-11-03	1.21593E+16	1.87E+11	940.84	1.95573E+25	1.95573E+19	9.57E-09	9.57
10	2021-12-03	5.20105E+15	8.00E+10	940.84	1.95573E+25	1.95573E+19	4.09E-09	4.09
11	2021-13-03	9.47916E+15	1.46E+11	940.84	1.95573E+25	1.95573E+19	7.46E-09	7.46
12	2021-15-03	3.33528E+15	5.13E+10	940.84	1.95573E+25	1.95573E+19	2.62E-09	2.62
13	2021-16-03	1.11029E+16	1.71E+11	940.84	1.95573E+25	1.95573E+19	8.73E-09	8.73
14	2021-17-03	1.29975E+16	2.00E+11	940.84	1.95573E+25	1.95573E+19	1.02E-08	10.22
15	2021-18-03	1.24895E+16	1.92E+11	940.84	1.95573E+25	1.95573E+19	9.82E-09	9.82
16	2021-19-03	1.0046E+16	1.55E+11	940.84	1.95573E+25	1.95573E+19	7.90E-09	7.90
17	2021-20-03	7.96947E+15	1.23E+11	940.84	1.95573E+25	1.95573E+19	6.27E-09	6.27
18	2021-21-03	1.36655E+16	2.10E+11	940.84	1.95573E+25	1.95573E+19	1.07E-08	10.75
19	2021-22-03	9.46102E+15	1.46E+11	940.84	1.95573E+25	1.95573E+19	7.44E-09	7.44
20	2021-30-03	6.4976E+15	1.00E+11	940.84	1.95573E+25	1.95573E+19	5.11E-09	5.11
21	2021-31-03	2.74936E+15	4.23E+10	940.84	1.95573E+25	1.95573E+19	2.16E-09	2.16
22	2021-01-04	4.27764E+15	6.58E+10	940.84	1.95573E+25	1.95573E+19	3.36E-09	3.36
23	2021-02-04	4.69884E+15	7.23E+10	940.84	1.95573E+25	1.95573E+19	3.70E-09	3.70
24	2021-03-04	9.84191E+15	1.51E+11	940.84	1.95573E+25	1.95573E+19	7.74E-09	7.74

Figure 8:*Calculation of vertical mixing ratios*

3.8. Comparison of ground-level measurements with satellite observations:

Tropospheric monitoring instrument (TROPOMI) and Ozone monitoring instrument (OMI) observations were used for the validation of satellite observations and comparison with ground-level measurements. Google Earth Engine was used to extract values of TROPOMI while GIOVANNI was used to get OMI measurements at the study site (33.6479° N, 72.9896° E). The ground-based MAX-DOAS and Conventional analyzers were mounted at the same coordinates. Both ground-level values and Satellite observations were compared for validation purposes.

3.9. Error Analysis:

Error analysis between the measurements of various instruments was performed by finding the root mean square error (RMSE) and the mean absolute error (MAE) given by Eqs. (22) and (23), respectively.

$$RMSE = \sqrt{\frac{1}{n}\sum_{i=1}^{n}\left(X_{(A)i} - X_{(M\ or\ S)i}\right)^2} \quad (22)$$

$$MAE = \frac{1}{n}\sum_{i=1}^{n}\left|X_{(A)i} - X_{(M\ or\ S)i}\right| \quad (23)$$

where n is the number of observations and X_A is for analyzer values and $X_{M\ or\ S}$ shows MAX-

DOAS or satellite values in either case for which the analysis is being performed. Besides computing differences in averages, overestimation or underestimation of values by instruments can be quantified by calculating the mean bias (MB), which is given by Eq. (24):

$$MB = \frac{1}{n}\sum_{i=1}^{n}\left(X_{(A)i} - X_{(M\ or\ S)i}\right) \quad (24)$$

where again n is the number of observations and X_A is for analyzer values and $X_{M\ or\ S}$ shows MAX-DOAS or satellite values in either case for which the analysis is being performed

3.10. Software used for Research Work:

The estimation and plotting of trace gasses required the use of various software as presented in Table 3:

Table 3:*The software's used in this study*

Sr. No.	Software	Purpose
1	Differential Optical Absorption Spectroscopy Intelligent System (DOASIS)	Operating Software for Max-DOAS and measurement of backscatter intensities
2	Windows Differential Optical Absorption Spectroscopy (WinDOAS)	For Convolution and Calibration
3	QDOAS	Analysis of UV-visible Spectra to retrieve dSCDs
4	Google Earth Engine	For retrieval of TROPOMI data
5	GIOVANNI	For retrieval of OMI data
6	Python	For retrieval of Boundary layer height
7	Microsoft Excel (v 2019)	Mathematical Calculations for tropospheric VCD extraction and Graphical representations

Chapter 4

RESULTS AND DISCUSSION

4.1. Retrieval of ground-level NO_2 and O_3 by various methods:

MAX-DOAS, OMI and TROPOMI ground level NO_2 measurements from September 2015 to September 2019 are shown in Fig. 9. It shows that most of the daily NO_2 measurements are higher during the winter season while values are lower during the summer season. This is mainly because of the meteorological conditions as during winter there is restricted movement and convection of atmospheric pollutants while there is no such atmospheric condition exists during summer and more convection and free movements of atmospheric pollutants occur. Relative change of the measurements for this time series shows overall decreasing trend with 26.67, 40 and 12 % for MAX-DOAS, TROPOMI and OMI respectively.

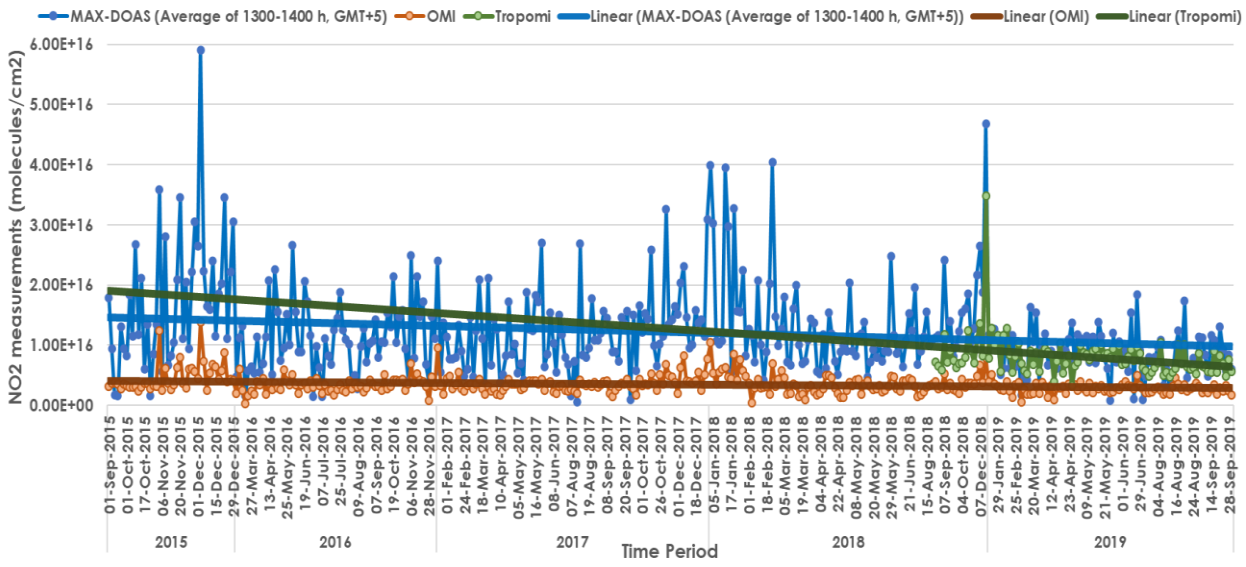

Figure 9:*MAX-DOAS, OMI and TROPOMI ground level NO_2 measurements from September 2015 to September 2019*

Figure 10 shows the hourly Diurnal of MAX-DOAS NO_2 measurements (6am-6pm) for the study

period. The concentrations shown an increasing trend during early hours of the day with a subsequent decrease in later part of the day. The 24-hourly Diurnal cycle of in situ NO_2 measurements is presented in Fig. 11. It shows higher concentrations during night hours with a decreasing trend from early to later part of the day. The minimum value is observed around 3 PM While maximum around 10 pm

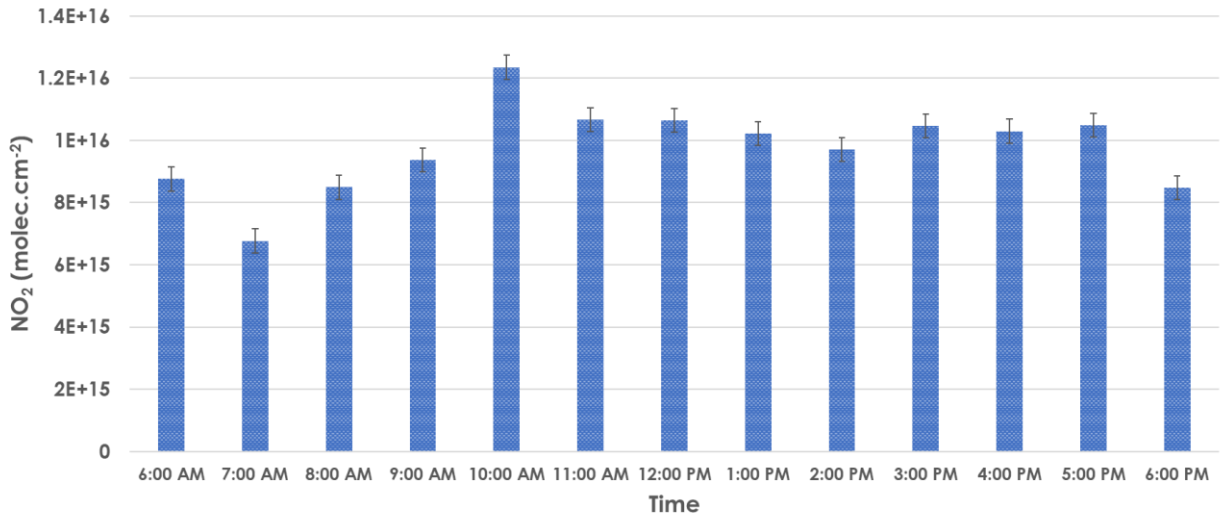

Figure 10:*Hourly Diurnal of MAX-DOAS NO_2 measurements for the study period*

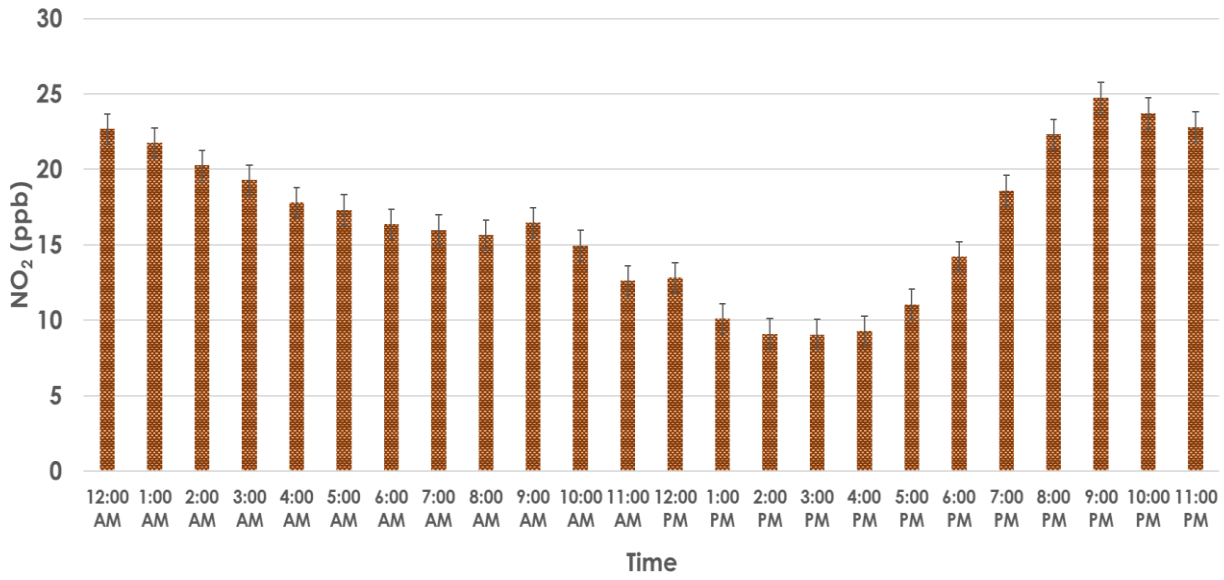

Figure 11:*Hourly Diurnal of in situ NO_2 measurements for the study period*

Figure 12 shows the MAX-DOAS Tropospheric O_3 measurements from March 2015-March 2019. It shows that highest values were observed during the warmer months, corresponding to

the observed columns of ozone. Figure 13 shows the hourly Diurnal of in situ O_3 measurements (6am-6pm). The 24-hourly Diurnal of in situ O_3 measurements for the study period is shown in Fig. 14. The values were lower during night and early part of the day with an increasing trend as the day progresses and then again it shows decreasing trend towards the end of the day. Figure 15 depicts the 24-hourly trend of NO_2 and O_3 in comparison. Both have shown opposite trend as NO_2 is a precursor of Ozone formation in the presence of VOCs and sunlight. Therefore, during hours of strong sunlight a dip in NO_2 values while a rise in O_3 concentrations is observed. The Pearson correlation also showed a strong opposite relation with r = -0.88.

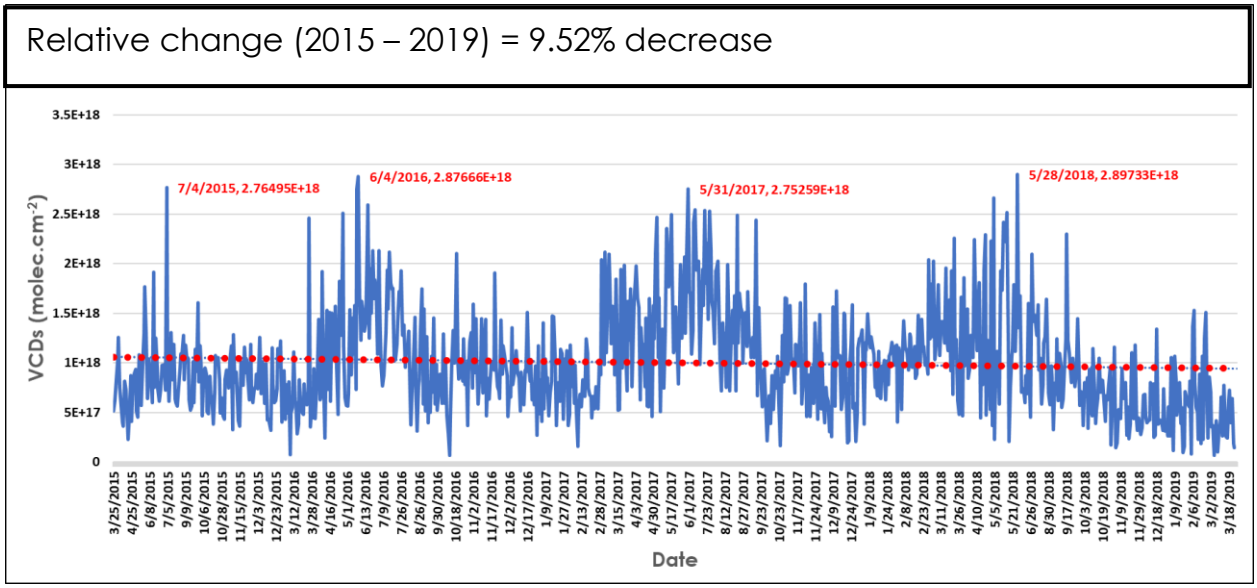

Figure 12:*MAX-DOAS O_3 Tropospheric measurements from March 2015-March 2019*

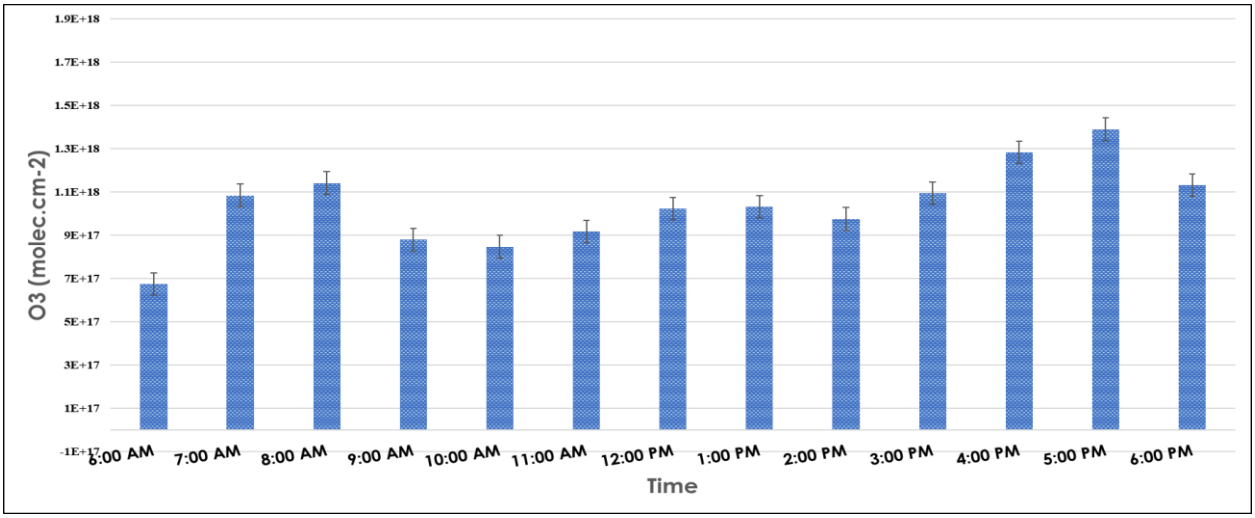

Figure 13:*Hourly Diurnal of MAX-DOAS O_3 measurements for the study period*

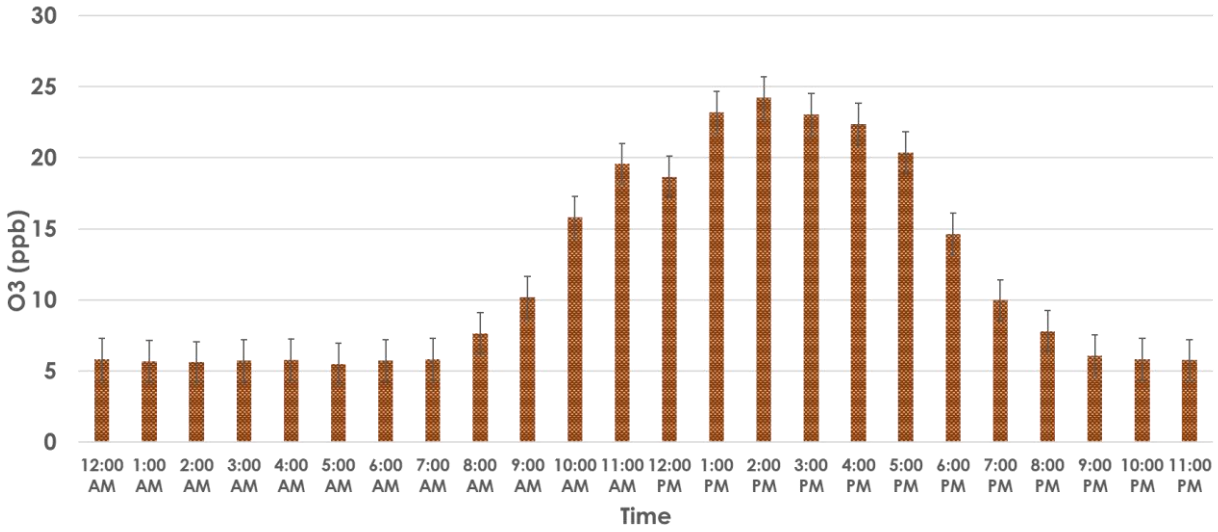

Figure 14:*Hourly Diurnal of in situ O_3 measurements for the study period*

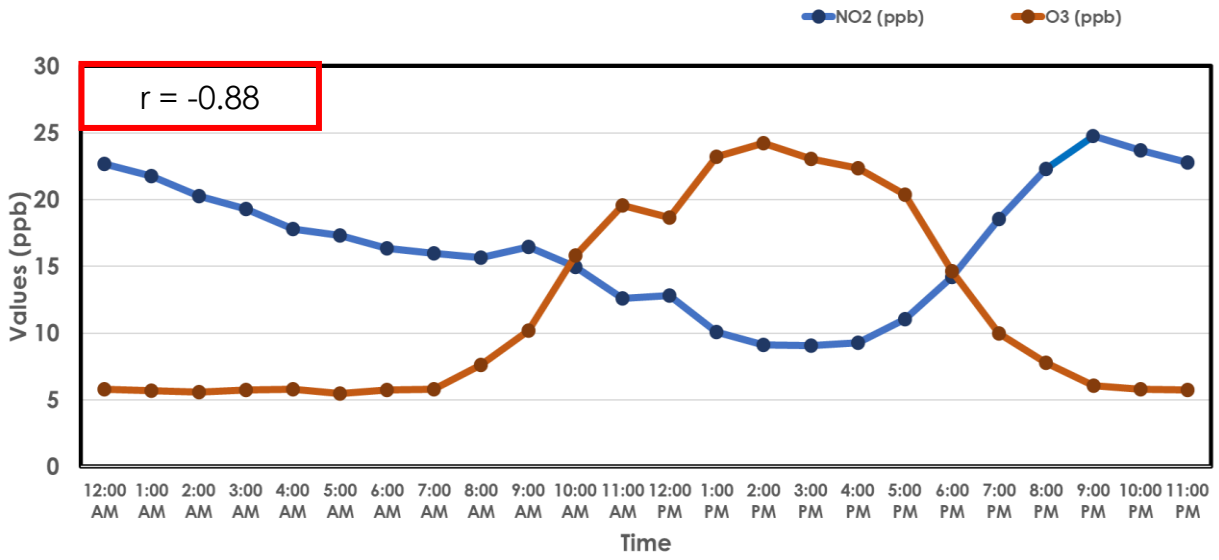

Figure 15:*Comparison of Hourly Diurnal of in situ NO_2 and O_3 measurements for the study period*

The vertical mixing ratios (ppbv) were obtained from the retrieved ground-level NO_2 by MAX-DOAS for the study period. The NO_2 measurements for the same period were also measured by the conventional analyzer. The values obtained from both instruments were compared for validation purposes.

4.2. Validation of ground-based and satellite instruments

The vertical mixing ratios (ppbv) were obtained from the retrieved ground-level NO_2 by MAX-DOAS for the study period. The NO_2 measurements for the same period were also measured by

the conventional analyzer. The values obtained from both instruments were compared for validation purposes.

4.2.1. Comparison of daily in situ measurements and MAX-DOAS vertical mixing ratios (VMRs)

The comparison of daily in situ measurements and MAX-DOAS vertical mixing ratios (VMRs) is presented in Fig. 16 and 17. Figure 16 shows a comparison between a daily average of MAX-DOAS NO_2 VMRs at 650 m an altitude (an average BLH) and in situ NO_2 measurements. The NO_2 concentrations have shown a similar trend for both MAX-DOAS and conventional analyzer. The NO_2 VMRs at an average BLH have shown higher values than the conventional analyzer. Further, to check the effective mixing height of NO_2, the comparison of a daily average of MAX-DOAS NO_2 VMRs at 300 m altitude and in situ NO_2 measurements is shown in Fig. 17. It also depicts a similar trend of NO_2 for both instruments but the values are synchronized with each other. *Zhang et al. (2016)* observed an altitude of 300 m as a reliable height in the boundary layer for well mixing of NO_2 and found decreasing trend from 300 m to the average BLH. Furthermore, NO_2 is a short-lived pollutant having a closely aligned distribution with combustion sources i.e., fossil fuels (Crawford et al., 2016).

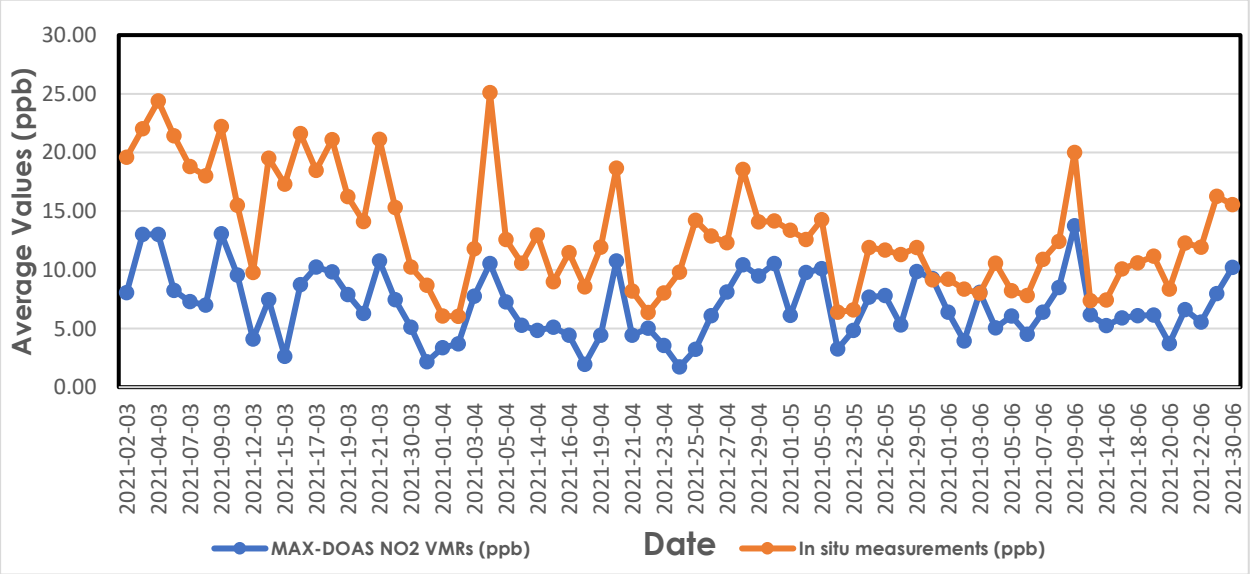

Figure 16:*Comparison of a daily average of MAX-DOAS NO2 VMRs at 650 m (average BLH) and in situ NO_2 measurements*

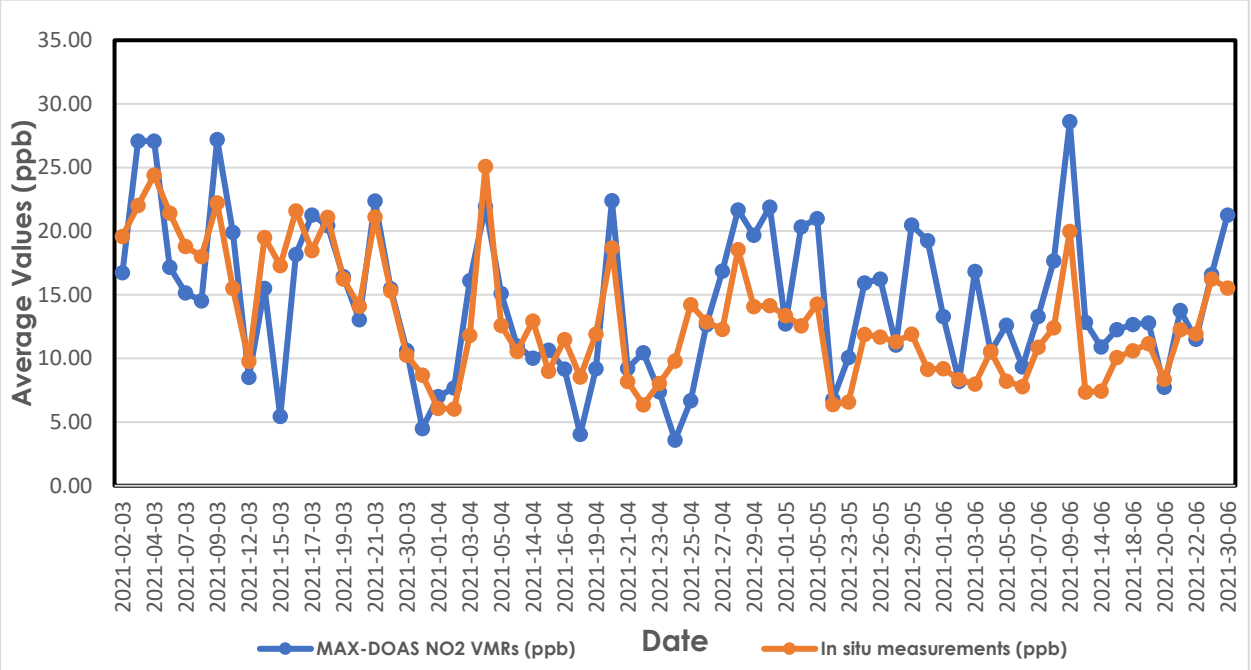

Figure 17:*Comparison of a daily average of MAX-DOAS NO_2 VMRs at 300 m and in situ NO_2 measurements*

4.2.2. Error analysis

Root mean square error (RMSE), Mean average error (MAE) and Mean Bias (MB) were calculated as part of the error analysis for checking the synchronization of NO_2 mixing ratios at an average BLH and 300 m altitude with the conventional analyzer. RMSE, MAE and MB between in situ measurements and MAX-DOAS VMRs at average BLH and 300 m altitude are presented in Fig. 18. It shows that RMSE between in situ measurements and MAX-DOAS VMRs at an altitude of 300 m is 4.36 ppb while it is 7.79 ppb for VMRs of an average BLH. Figure 18 also shows MAE between in situ measurements and MAX-DOAS VMRs at an altitude of 300 m which is 3.47 ppb while it is 6.93 ppb for VMRs of an average BLH. MB is also presented in Fig. 18 between in situ measurements and MAX-DOAS VMRs at an altitude of 300 m which is -0.72 ppb while it is 6.92 ppb for VMRs of an average BLH. Here, the negative sign indicates that NO_2 VMRs were underestimated by MAX-DOAS at an altitude of 300 m. All the error analysis supports that the NO_2 values of in situ measurements and MAX-DOAS VMRs at an altitude of 300 m from the study site are more synchronized with each other than VMRs of MAX-

DOAS at an average BLH for this season. It is pertinent to note that an altitude of 300 m at the study site for this season is an effective mixing height of NO_2.

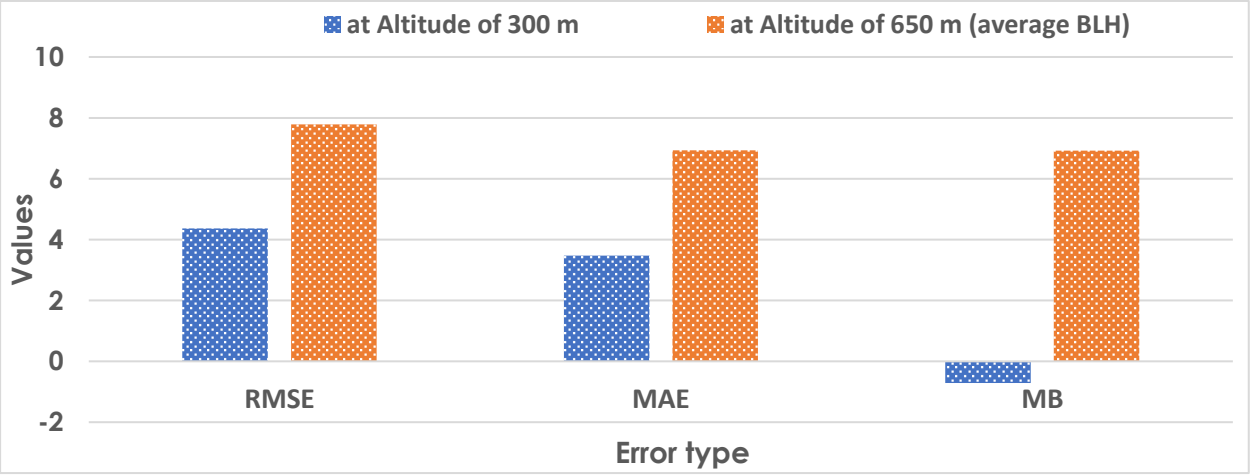

Figure 18:*RMSE, MAE and MB between MAX-DOAS VMRs and in situ measurements*

4.2.3. Regression analysis:

Furthermore, the linear regression analysis was performed to check the correlation between the two instruments. A linear correlation plot was drawn between in situ measurements and MAX-DOAS VMRs as shown in Fig. 19. The data from both instruments have shown a good positive correlation with $R^2 = 0.53$ (r = 0.73) which depicts a good agreement between MAX-DOAS and conventional analyzer for NO_2 measurements.

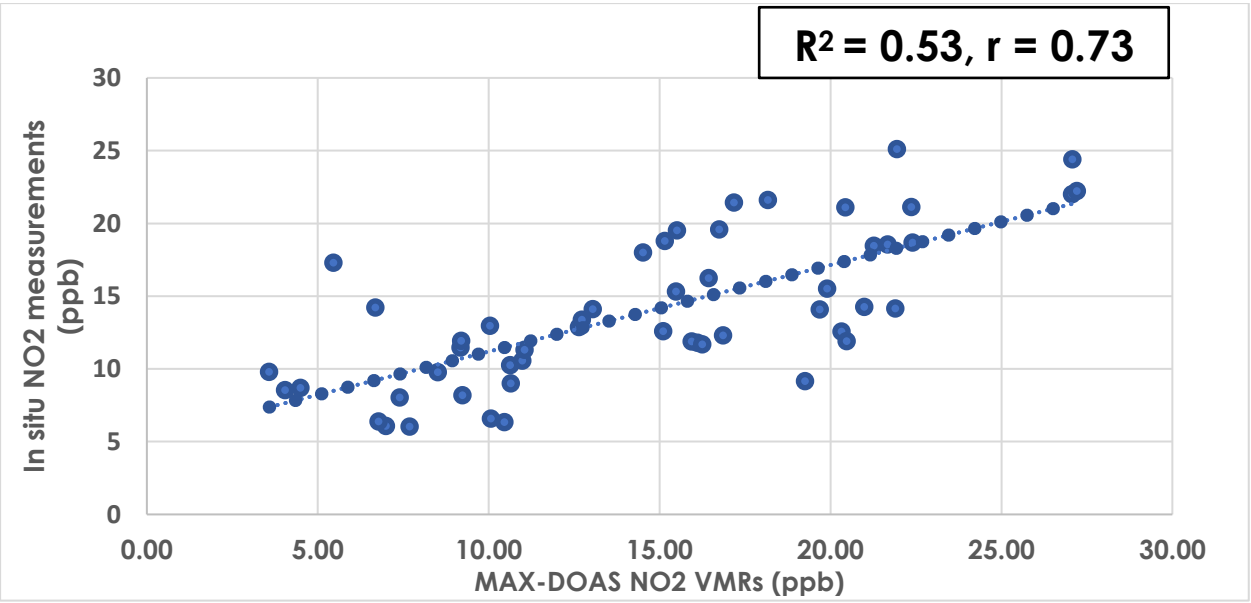

Figure 19:*MAX-DOAS NO_2 VMRs vs in situ NO_2 measurements*

4.2.4. Retrieval of ground-level O_3 by MAX-DOAS and its validation with Conventional analyzer

The validation of ground-level O_3 VMRs by MAX-DOAS with O_3 measurements of Conventional analyzer was investigated. Figure 20 shows comparison of MAX-DOAS O_3 VMRs at 650 m (average BLH) and in situ O_3 measurements. It was found that Mini MAX-DOAS was not been able to differentiate between tropospheric and stratospheric O_3 concentrations due to its sensitivity constraints for ground-level O_3. It is mainly because of the concentration of O_3 in the stratosphere is normally about 1 order of magnitude higher than that in the troposphere. Therefore, the retrieval of ground-level O_3 from MAX-DOAS observations is still a challenge due to interference of the stratospheric O_3 absorption (Hendrick et al., 2011).

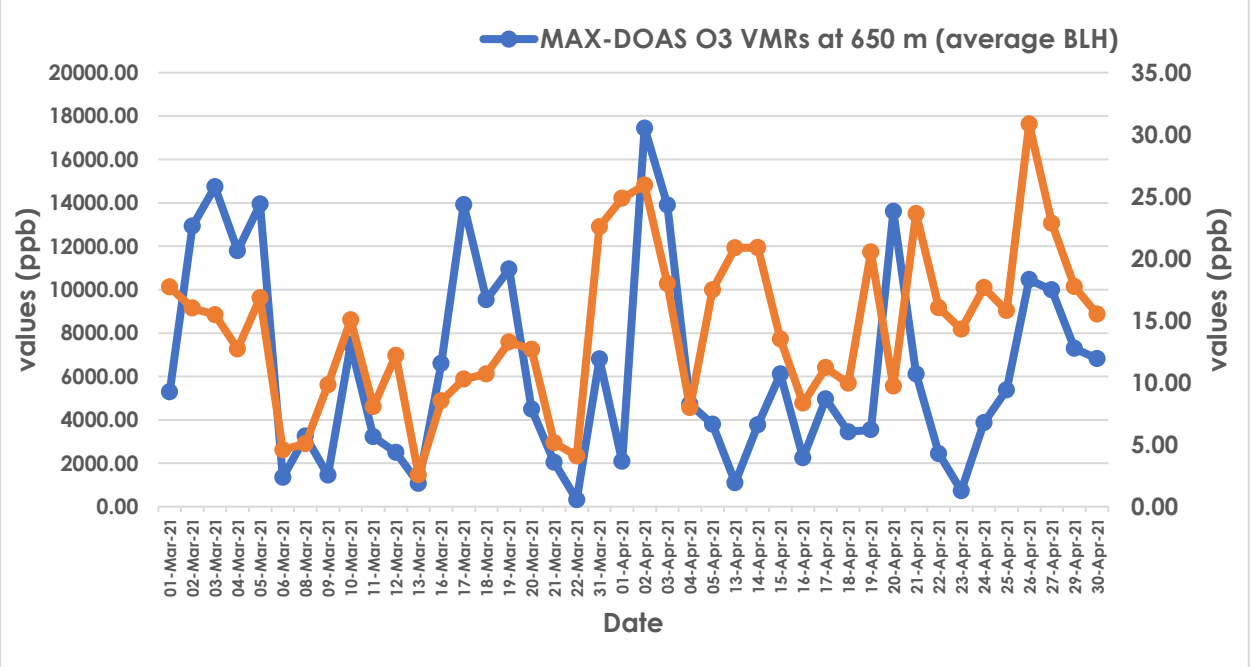

Figure 20:*Comparison of MAX-DOAS O_3 VMRs at 650 m (average BLH) and in situ O_3 measurements*

4.2.5. Comparison of ground-level measurements with satellite observations

Ground-based NO_2 values were compared with TROPOMI (having a resolution of 7 x 3.5 km) and OMI (having a resolution of 13 x 24 km) measurements for validation of satellite observations. The ground-based measurements were averaged for one hour time period from 1300-1400 hours local time (UTC

0800-0900 hours) as the satellite (TROPOMI and OMI) overpass time in the study area is around 1330 hours local time (UTC 0830 hours). Figure 21 shows the comparison of MAX-DOAS, TROPOMI and OMI NO_2 VMRs at an altitude of 650 m (an average BLH) and in situ NO_2 measurements. The NO_2 concentrations have shown a similar trend for both ground-based measurements and satellite observations but quantitatively they have shown less agreement. Further, the Comparison of MAX-DOAS, TROPOMI and OMI NO_2 VMRs at an altitude of 300 m and in situ measurements is shown in Fig. 22. It depicts a similar trend of NO_2 measurements but quantitatively a better agreement is observed among various instruments for this altitude. *Zhang et al. (2016)* observed an altitude of 300 m as a reliable height in the boundary layer for well mixing of NO_2 and found decreasing trend from 300 m to the average BLH. Furthermore, NO_2 is a short-lived pollutant having a closely aligned distribution with combustion sources i.e., fossil fuels (Crawford et al., 2016).

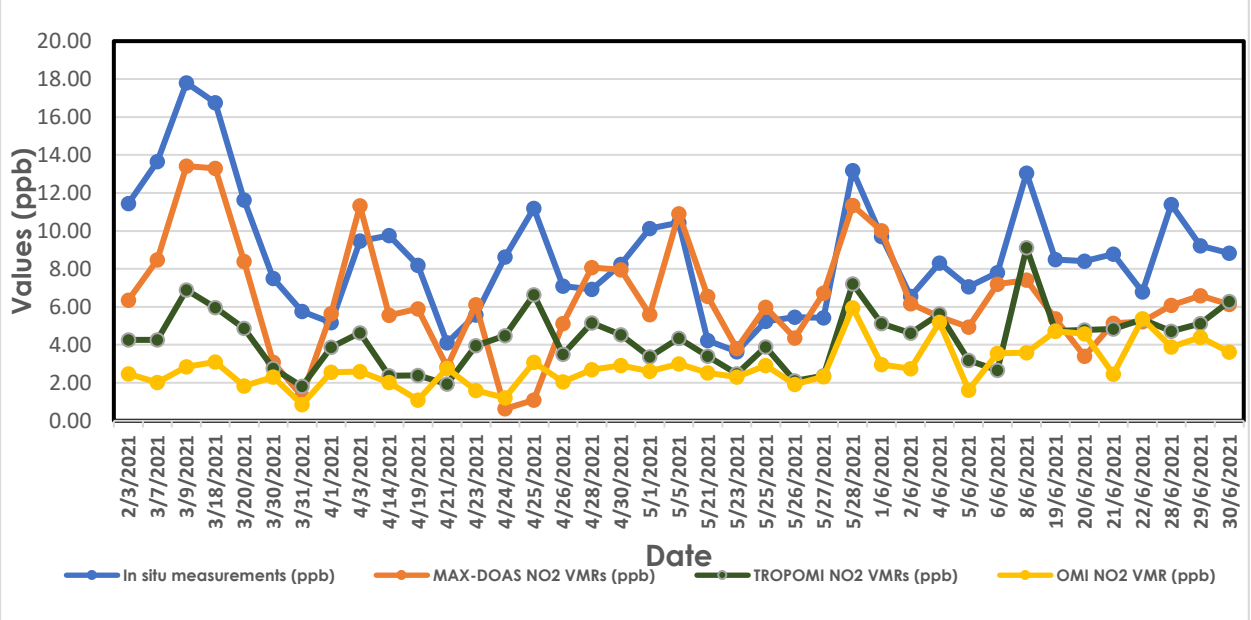

Figure 21:*Comparison of MAX-DOAS, TROPOMI and OMI NO_2 VMRs at 650 m (average BLH) and in situ measurements*

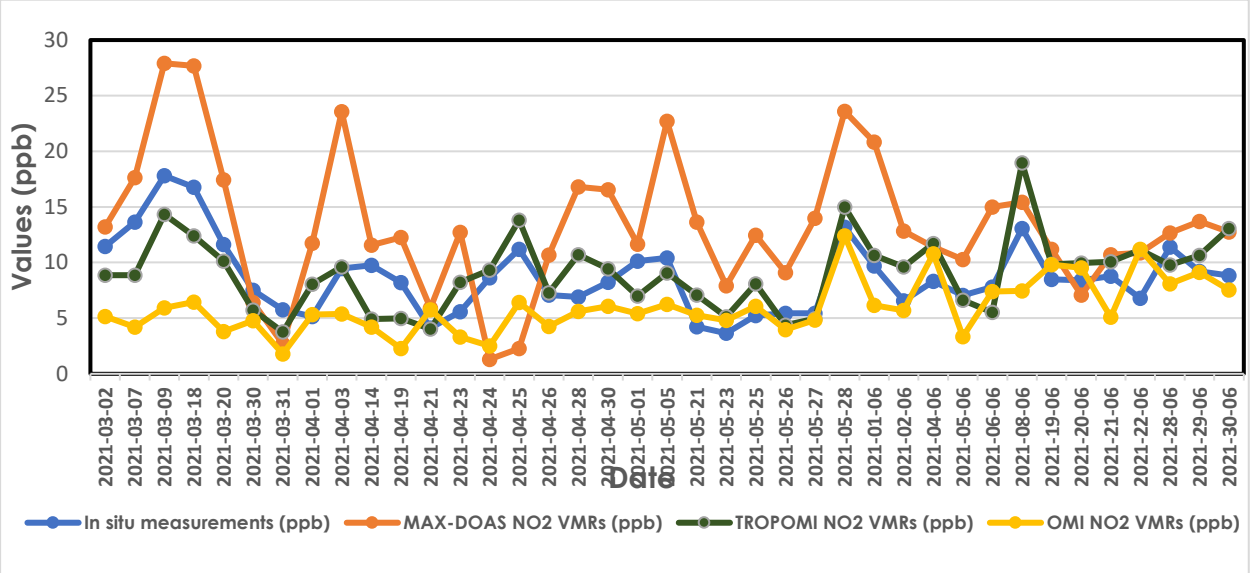

Figure 22:*Comparison of MAX-DOAS, TROPOMI and OMI NO_2 VMRs at 300 m and in situ measurements*

Figure 23 represents the Instruments sensitivity and various atmospheric divisions. In Troposphere, the average BLH for the study period is 650 m while the effective NO_2 mixing height is 300 m. The in-situ measurements are representatives up to 5m while MAX-DOAS visibility range is up to 5-7 km in Troposphere. It is important to note that the satellite measurements are columnar observations and they are sensitive to variations in boundary layer height and challenged in their sensitivity to changes in ground-based measurements. Vertical profiles of NO_2 and O_3 by *Zhang et al. 2016* are presented in Fig. 24. NO_2 profiles are mainly within the BLH which shows that it is a short-lived pollutant having a closely aligned distribution with its sources i.e., fossil fuels. While O3 profiles shown relatively more vertical distribution.

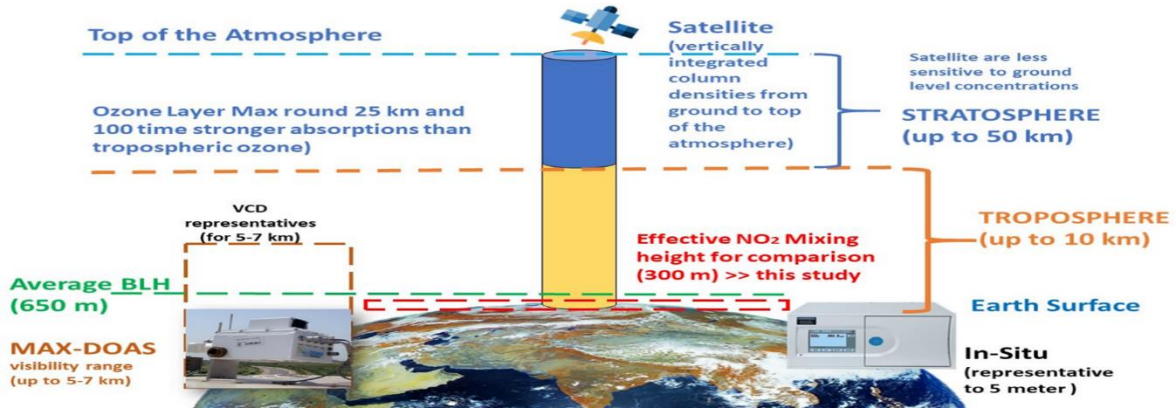

Figure 23:*Instruments sensitivity in various atmospheric divisions*

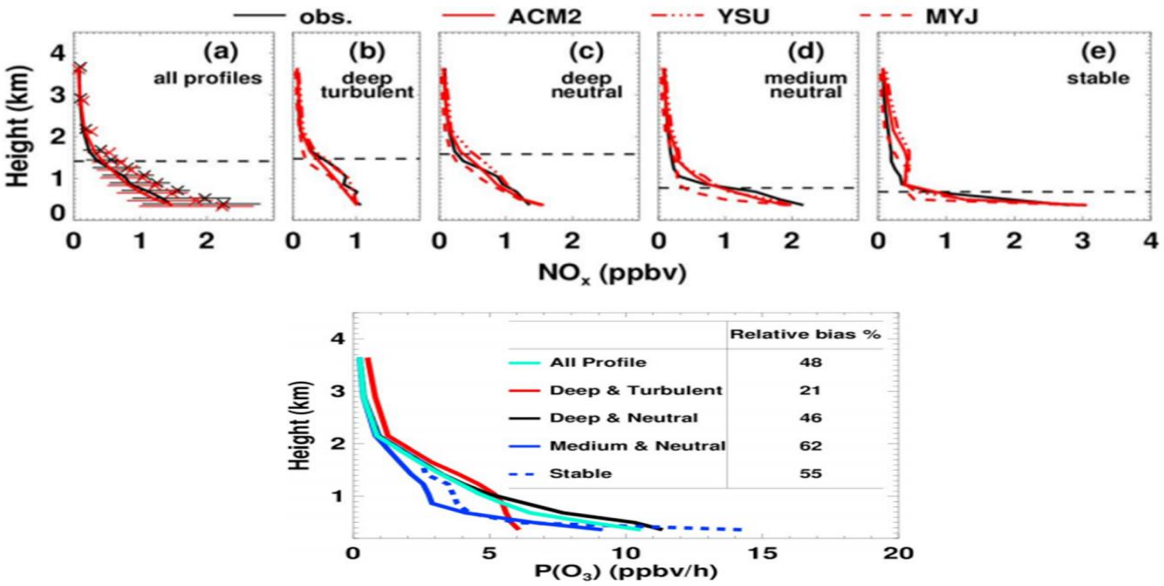

Figure 24:*Vertical profiles of NO_2 and O_3 (adopted from Zhang et al. 2016)*

4.2.6. Error analysis

Error analysis was performed to check the better agreement among ground-based measurements and satellite observations for different altitudes i.e., at 300 m and 650 m (an average BLH). The in situ measurements and TROPOMI VMRs were identified for this analysis as being an independent NO_2 measurement technique, these two have shown a better and improved agreement identified by linear regression analysis i.e., r = 0.72. Root mean square error (RMSE), Mean average error (MAE) and Mean Bias (MB) were calculated as part of the error analysis. RMSE, MAE and MB between ground-based in situ measurements and satellite VMRs at 300 m altitude and average BLH are presented in Fig. 25. It shows that RMSE between ground measurements and satellite VMRs at 300 is 2.97 ppb while it is 5.74 ppb for VMRs for an average BLH. Figure 25 also shows MAE between ground measurements and satellite VMRs at an altitude of 300 m that is 2.45 ppb while it is 4.98 ppb for VMRs for an average BLH. Mean bias (MB) is also presented in Fig. 25 between ground measurements and satellite VMRs at an altitude of 300 m that is 0.60 ppb while it is 4.98 ppb for VMRs for an average BLH. Again, analysis supports that the NO_2 values of ground measurements and satellite VMRs at an altitude of 300 m from the study site are more synchronized than satellite VMRs at an average BLH for this season.

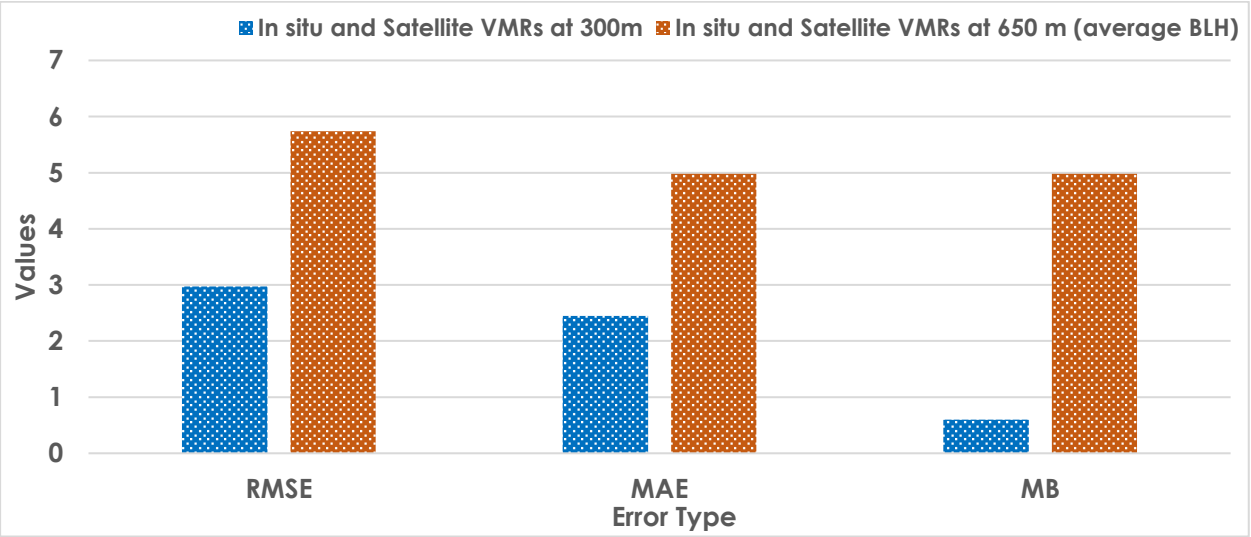

Figure 25:*Comparison of RMSE, MAE and MB between in situ measurements and Satellite VMRs*

4.2.7. Regression analysis

Furthermore, the linear regression analysis was performed to check the correlation between values of conventional analyzer and satellite VMRs. The same was performed for VMRs of ground-based MAX-DOAS and satellite VMRs. A linear correlation plot has been shown in Fig. 26 between the conventional analyzer and satellite VMRs. The data from both instruments have shown a good positive correlation with R^2 = 0.52 (r = 0.72) which depicts a good agreement between the two instruments. The linear correlation plot presented in Fig. 27 shows a correlation between MAX-DOAS and satellite VMRs. The data from these instruments have also shown a good positive correlation with R^2 = 0.74 (r = 0.86) which depicts a good agreement between MAX-DOAS and satellite VMRs. It is pertinent to note that these two have shown an improved correlation mainly because ground-based MAX-DOAS and satellite (TROPOMI) are using the same technique i.e., DOASIS for the retrieval of NO_2 values. Furthermore, the linear regression of in situ measurements vs OMI VMRs, MAX-DOAS VMRs vs OMI VMRs and TROPOMI VMRs vs OMI VMRs is presented in Fig. 28, 29 and 30 respectively. The in situ measurements and OMI VMRs have shown a moderate correlation with R^2 = 0.30 (r = 0.54). It is mainly because of the coarse resolution and a larger pixel size of OMI i.e., 13 x 24 km. It could be also partially because two instruments are using independent NO_2 measurement techniques. Mini MAX-DOAS VMRs and OMI VMRs have shown a strong positive correlation with R^2 = 0.50 (r = 0.70). Furthermore, the TROPOMI VMRs and OMI VMRs have

also shown a strong positive correlation with $R^2 = 0.51$ (r = 0.71).

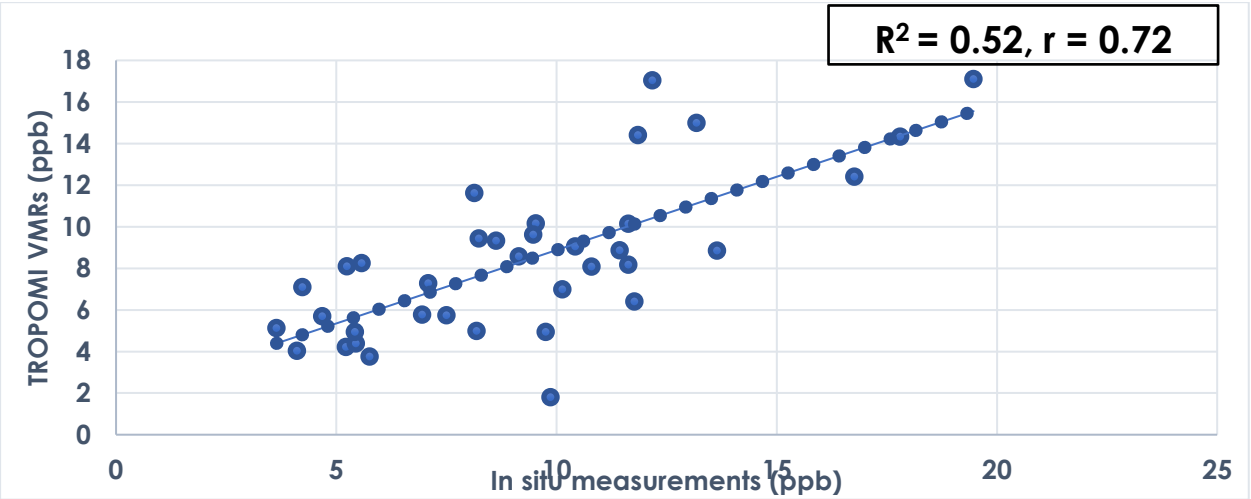

Figure 26:*In situ measurements vs TROPOMI VMRs*

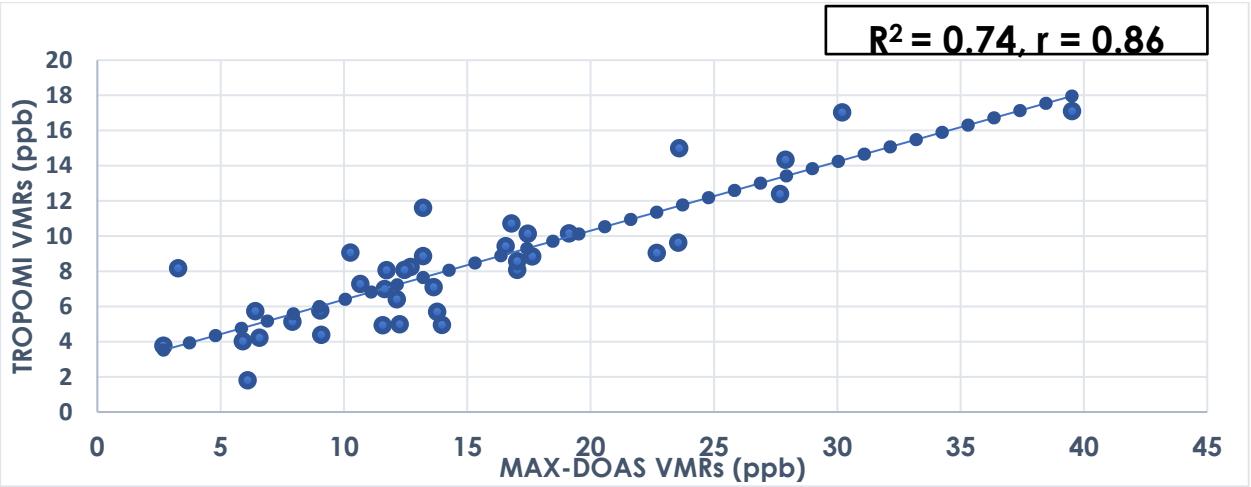

Figure 27:*MAX-DOAS vs TROPOMI VMRs*

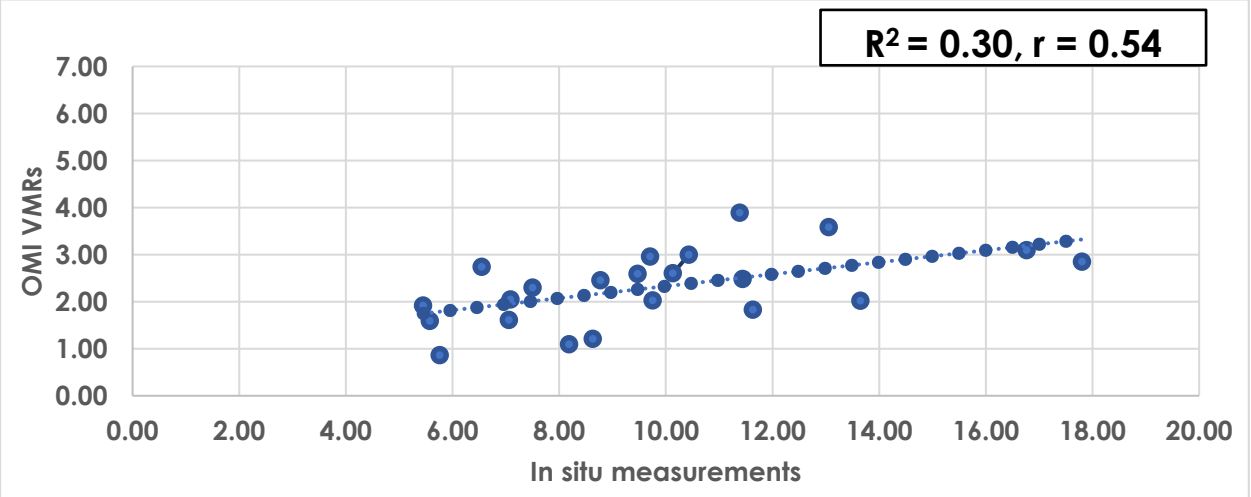

Figure 28:*In situ vs OMI VMRs*

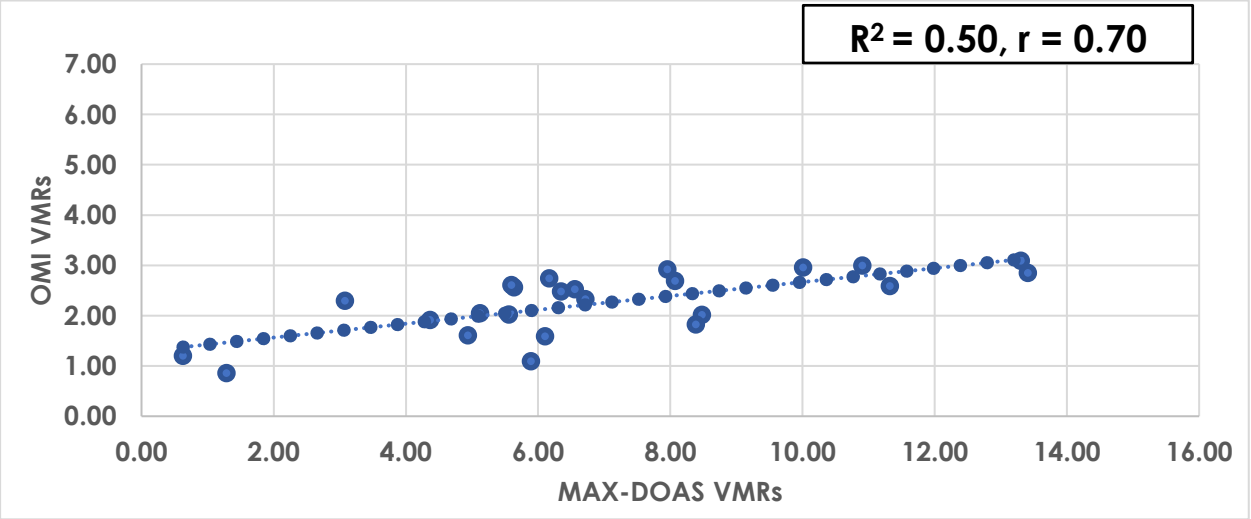

Figure 29:*MAX-DOAS VMRs vs OMI VMRs*

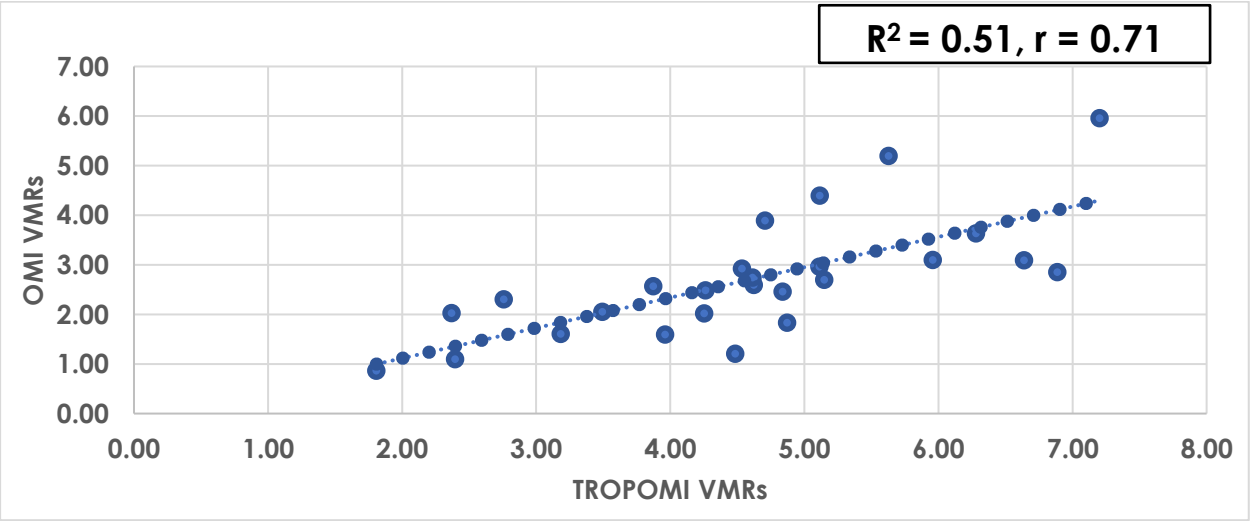

Figure 30:*TROPOMI VMRs vs OMI VMRs*

4.2.8. Validation outcomes

The validation outcomes showed that NO_2 is a good candidate for validation while O_3 is not a good candidate for validation. In order to have appropriate validation, one should keep in mind following aspects:

1. The sensitivity of each instrument
2. Vertical profile of target specie
3. Role of BLH and other meteorological conditions

Chapter 5

CONCLUSION and RECOMMENDATIONS

5.1. Conclusion

In this study, ground level NO_2 and O_3 concentrations were retrieved and the validation for VMRs of Multi-Axis Differential Optical Absorption Spectroscopy (Mini MAX-DOAS) vertical column densities (VCDs) with measurements of conventional analyzers and comparison of ground-based and satellite observations for NO_2 and O_3 is presented. The daily NO_2 measurements were higher during the winter season while values were lower during the summer season. The retrieved O_3 concentrations has shown highest values during the warmer months, corresponding to the observed columns of ozone. The comparison of NO_2 has shown a similar trend for VMRs of both altitudes i.e., 300 m and 650 m (average BLH) with conventional analyzer but values at 300 m altitude have shown greater agreement as less errors detected for these VMRs. The RMSE, MAE was 4.36 ppb and 3.47 ppb respectively for an altitude of 300 m while they were 7.79 ppb and 6.93 ppb for an average BLH. The MB for an altitude of 300 m was -0.72 ppb and 6.92 ppb for an average BLH. Here, the negative sign indicates that NO_2 VMRs were underestimated slightly by Mini MAX-DOAS at an altitude of 300 m. All the error analysis supported that the NO_2 values of in situ measurements and MAX-DOAS VMRs at an altitude of 300 m from the study site are more synchronized with each other than VMRs of MAX-DOAS at an average BLH for this season. It is pertinent to note that an altitude of 300 m at the study site for this season is an effective mixing height of NO_2 because of its shorter lifetime in the atmosphere. The relative difference of measured values by instruments for the study period have shown a decreasing trend. Furthermore, the linear regression analysis for values of both instruments has shown a strong positive correlation for NO_2 with $r = 0.73$.

Similar validation was performed for O_3 measurements but investigated that Mini MAX-DOAS

was not been able to differentiate between tropospheric and stratospheric O_3 concentrations due to its sensitivity constraints for ground-level O_3. It has shown very high O_3 VMRs as these are not possible in troposphere. The fraction of O_3 in the stratosphere is usually higher than that in the troposphere. Therefore, the retrieval of ground-level O_3 from Mini MAX-DOAS observations is still a challenge due to interference of the stratospheric O_3 absorption.

Furthermore, the ground-based NO_2 measurements were compared with satellite observations (TROPOMI and OMI VMRs) for both altitudes i.e., at 300 m and an average BHL. Here, the ground measurements and satellite observations have shown a similar trend for both altitudes. The error analysis again presented that VMRs of TROPOMI at an altitude of 300 m were more synchronized with ground-based measurements. Through linear regression analysis, it was identified that the ground measurements and TROPOMI observations have shown a strong positive correlation with $r = 0.72$ and $r = 0.86$ for conventional analyzer vs TROPOMI and Mini MAX-DOAS vs TROPOMI respectively. Furthermore, the Pearson correlation (r) of in situ measurements vs OMI VMRs, MAX-DOAS VMRs vs OMI VMRs and TROPOMI VMRs vs OMI VMRs was 0.54, 0.70 and 0.71 respectively.

5.2. Recommendations

1. More robust and long-term study needs to be conducted to understand the nature of effective vertical mixing height of NO_2 for all seasons in other geophysical locations.

2. More studies to be conducted for exploring the cost-effective options in terms of low-cost sensors to monitor ground-level Ozone.

3. All pollutants strategy to be investigated for understanding the interdependence of various air pollutants in local conditions.

4. An air monitoring network needs to be set-up across Pakistan at the earliest to explore the nature and behavior of various pollutants across the country.

References

Badr, O., & Probert, S. J. A. e. (1993). Oxides of nitrogen in the earth's atmosphere: trends, sources, sinks and environmental impacts. *46*(1), 1-67.

Bang, H. Q., Nguyen, H. D., Vu, K., Hien, T. T. J. E. M., & Assessment. (2018). Photochemical Smog Modelling Using the Air Pollution Chemical Transport Model (TAPM-CTM) in Ho Chi Minh City, Vietnam. 1-16.

Beard, B. A., & Freas, W. P. J. E. S. A. F. (1994). National Air Quality and Emissions Trends Report. *163*.

Beelen, R., Hoek, G., Vienneau, D., Eeftens, M., Dimakopoulou, K., Pedeli, X., . . . Marcon, A. J. A. E. 2013). Development of NO2 and NOx land use regression models for estimating air pollution exposure in 36 study areas in Europe–The ESCAPE project. *72*, 10-23.

Beirle, S., Platt, U., Wenig, M., Wagner, T. J. A. C., & Physics. (2003). Weekly cycle of NO 2 by GOME measurements: A signature of anthropogenic sources. *3*(6), 2225-2232.

Bobrowski, N., Hönninger, G., Galle, B., & Platt, U. J. N. (2003). Detection of bromine monoxide in a volcanic plume. *423*(6937), 273.

Brasseur, G. P., & Solomon, S. (2006). *Aeronomy of the middle atmosphere: chemistry and physics of the stratosphere and mesosphere* (Vol. 32): Springer Science & Business Media.

Brook, R. D., Brook, J. R., Urch, B., Vincent, R., Rajagopalan, S., & Silverman, F. J. C. (2002). Inhalation of fine particulate air pollution and ozone causes acute arterial vasoconstriction in healthy adults. *105*(13), 1534-1536.

Burrows, J. P., Platt, U., & Borrell, P. (2011). *The remote sensing of tropospheric composition from space: Springer Science & Business Media*.

Chan, K., Hartl, A., Lam, Y., Xie, P., Liu, W., Cheung, H., . . . Xu, J. J. A. E. (2015). Observations of tropospheric NO2 using ground based MAX-DOAS and OMI measurements during the Shanghai World Expo 2010. *119*, 45-58.

Chan, K., Wiegner, M., Wenig, M., & Pöhler, D. J. S. o. t. t. e. (2018). Observations of tropospheric aerosols and NO2 in Hong Kong over 5 years using ground based MAX-DOAS. *619*, 1545- 1556.

Chan, K. L., Wang, Z., Ding, A., Heue, K.-P., Shen, Y., Wang, J., . . . Wenig, M. J. A. C. P. D. (2019). MAX-DOAS measurements of tropospheric NO 2 and HCHO in Nanjing and the comparison to OMI observations.

Chen, X., Wang, F., Hyun, J. Y., Wei, T., Qiang, J., Ren, X., . . . Yoon, J. J. C. S. R. (2016). Recent progress in the development of fluorescent, luminescent and colorimetric probes for detection of reactive oxygen and nitrogen species. *45*(10), 2976-3016.

Cheng, S., Ma, J., Cheng, W., Yan, P., Zhou, H., Zhou, L., & Yang, P. J. J. o. E. S. (2019). Tropospheric NO2 vertical column densities retrieved from ground-based MAX-DOAS measurements at Shangdianzi regional atmospheric background station in China. *80*, 186-196.

Coburn, S., Dix, B., Sinreich, R., & Volkamer, R. J. A. M. T. (2011). The CU ground MAX-DOAS instrument: characterization of RMS noise limitations and first measurements near Pensacola, FL of BrO, IO, and CHOCHO. *4*(11), 2421-2439.

Demirel, G., Özden, Ö., Döğeroğlu, T., & Gaga, E. O. J. S. o. t. t. e. (2014). Personal exposure of primary school children to BTEX, NO2 and ozone in Eskişehir, Turkey: Relationship with indoor/outdoor concentrations and risk assessment. *473*, 537-548.

Dix, B., Koenig, T., & Volkamer, R. J. A. M. T. (2016). Parameterization retrieval of trace gas volume mixing ratios from Airborne MAX-DOAS. *9*(11).

Dockery, D. W., & Pope, C. A. J. A. r. o. p. h. (1994). Acute respiratory effects of particulate air pollution. *15*(1), 107-132.

Drummond, J. W., Volz, A., & Ehhalt, D. H. J. J. o. a. c. (1985). An optimized chemiluminescence detector for

tropospheric NO measurements. *2*(3), 287-306.
Finlayson-Pitts, B. J., & Pitts, J. N. J. S. (1997). Tropospheric air pollution: ozone, airborne toxics, polycyclic aromatic hydrocarbons, and particles. *276*(5315), 1045-1051.
Fioletov, V., McLinden, C., Krotkov, N., Yang, K., Loyola, D., Valks, P., … Chance, K. J. J. o. G. R. A. (2013). Application of OMI, SCIAMACHY, and GOME-2 satellite SO2 retrievals for detection of large emission sources. *118*(19), 11,399-311,418.
Fontijn, A., Sabadell, A. J., & Ronco, R. J. J. A. c. (1970). Homogeneous chemiluminescent measurement of nitric oxide with ozone. Implications for continuous selective monitoring of gaseous air pollutants. *42*(6), 575-579.
Grosjean, D., Harrison, J. J. E. s., & technology. (1985). Response of chemiluminescence NOx analyzers and ultraviolet ozone analyzers to organic air pollutants. *19*(9), 862-865.
Guenther, A., Geron, C., Pierce, T., Lamb, B., Harley, P., & Fall, R. J. A. E. (2000). Natural emissions of non-methane volatile organic compounds, carbon monoxide, and oxides of nitrogen from North America. *34*(12-14), 2205-2230.
Halla, J., Wagner, T., Beirle, S., Brook, J., Hayden, K., O'brien, J., . . . Physics. (2011). Determination of tropospheric vertical columns of NO 2 and aerosol optical properties in a rural setting using MAX-DOAS. *11*(23), 12475-12498.
Han, X., & Naeher, L. P. J. E. i. (2006). A review of traffic-related air pollution exposure assessment studies in the developing world. *32*(1), 106-120.
Hendrick, F., Müller, J.-F., Clémer, K., Wang, P., Mazière, M. D., Fayt, C., … Physics. (2014). Four years of ground-based MAX-DOAS observations of HONO and NO 2 in the Beijing area. *14*(2), 765-781.
Hilboll, A., Richter, A., Burrows, J. J. A. C., & Physics. (2013). Long-term changes of tropospheric NO2 over megacities derived from multiple satellite instruments. *13*(8), 4145.
Hong, Q., Xie, Z., Liu, C., Wang, F., Xie, P., Kang, H., . . . Physics. (2016). Speciated atmospheric mercury on haze and non-haze days in an inland city in China. *16*(21), 13807-13821.
Hönninger, G., Friedeburg, C. v., Platt, U. J. A. C., & Physics. (2004). Multi axis differential optical absorption spectroscopy (MAX-DOAS). *4*(1), 231-254.
Ibrahim, O. (2009). *Applications on Ground-based Tropospheric Measurements using Multi-Axis Differential Optical Absorption Spectrosopy*.
Irie, H., Kanaya, Y., Akimoto, H., Tanimoto, H., Wang, Z., Gleason, J., . . . Physics. (2008). Validation of OMI tropospheric NO 2 column data using MAX-DOAS measurements deep inside the North China Plain in June 2006: Mount Tai Experiment 2006. *8*(22), 6577-6586.
Jahangir, S., Ahmad, S. S., Aziz, N., Shah, M. T. A. J. J. o. I. E. A., & Science. (2013). Spatial variation of nitrogen dioxide concentration in private and public hospitals of Rawalpindi and Islamabad, Pakistan. *8*, 16-24.
Khan, W. A., Khokhar, M. F., Shoaib, A., & Nawaz, R. J. A. P. R. (2018). Monitoring and analysis of formaldehyde columns over Rawalpindi-Islamabad, Pakistan using MAX-DOAS and satellite observation. *9*(5), 840-848.
Khokhar, M., Naveed, S., Butt, J., & Abbas, Z. J. A. (2016). Comparative analysis of atmospheric glyoxal column densities retrieved from MAX-DOAS observations in Pakistan and during MAD-CAT field campaign in Mainz, Germany. *7*(5), 68.
Kreher, K., Van Roozendael, M., Hendrick, F., Apituley, A., Dimitropoulou, E., Frieß, U., . . . Ang, L. (2019). Intercomparison of NO2, O4, O3 and HCHO slant column measurements by MAX- DOAS and zenith-sky UV-Visible spectrometers during the CINDI-2 campaign.
Leser, H., Hönninger, G., & Platt, U. J. G. R. L. (2003). MAX-DOAS measurements of BrO and NO2 in the marine boundary layer. *30*(10).
Li, C., Zhang, Q., Krotkov, N. A., Streets, D. G., He, K., Tsay, S. C., & Gleason, J. F. J. G. R. L. (2010). Recent

large reduction in sulfur dioxide emissions from Chinese power plants observed by the Ozone Monitoring Instrument. *37*(8).
Li, X., Brauers, T., Hofzumahaus, A., Lu, K., Li, Y., Shao, M., . . . Physics. (2013). MAX-DOAS measurements of NO 2, HCHO and CHOCHO at a rural site in Southern China. *13*(4), 2133- 2151.
Lin, J.-T., Martin, R., Boersma, K., Sneep, M., Stammes, P., Spurr, R., . . . Physics. (2014). Retrieving tropospheric nitrogen dioxide from the Ozone Monitoring Instrument: effects of aerosols, surface reflectance anisotropy, and vertical profile of nitrogen dioxide. *14*(3), 1441-1461.
Lin, J.-T., McElroy, M. B. J. A. C., & Physics. (2011). Detection from space of a reduction in anthropogenic emissions of nitrogen oxides during the Chinese economic downturn. *11*(15), 8171-8188.
Liu, Q., Ma, T., Olson, M. R., Liu, Y., Zhang, T., Wu, Y., & Schauer, J. J. J. S. r. (2016). Temporal variations of black carbon during haze and non-haze days in Beijing. *6*, 33331.
Lohberger, F., Hönninger, G., & Platt, U. J. A. o. (2004). Ground-based imaging differential optical absorption spectroscopy of atmospheric gases. *43*(24), 4711-4717.
Lübken, F. J. J. J. o. G. R. A. (1999). Thermal structure of the Arctic summer mesosphere. *104*(D8), 9135-9149.
Ma, J., Beirle, S., Jin, J., Shaiganfar, R., Yan, P., Wagner, T. J. A. C., & Physics. (2013). Tropospheric NO 2 vertical column densities over Beijing: results of the first three years of ground-based MAX-DOAS measurements (2008–2011) and satellite validation. *13*(3), 1547-1567.
Martin, R. V. J. A. e. (2008). Satellite remote sensing of surface air quality. *42*(34), 7823-7843.
Pandey, J. S., Kumar, R., & Devotta, S. J. A. E. (2005). Health risks of NO2, SPM and SO2 in Delhi (India). *39*(36), 6868-6874.
Parekh, P. P., Khwaja, H. A., Khan, A. R., Naqvi, R. R., Malik, A., Shah, S. A., … Hussain, G. J. A. E. (2001). Ambient air quality of two metropolitan cities of Pakistan and its health implications. *35*(34), 5971-5978.
Peters, E., Wittrock, F., Großmann, K., Frieß, U., Richter, A., Burrows, J. J. A. C., & Physics. (2012). Formaldehyde and nitrogen dioxide over the remote western Pacific Ocean: SCIAMACHY and GOME-2 validation using ship-based MAX-DOAS observations. *12*(22), 11179-11197.
Pikelnaya, O., Hurlock, S. C., Trick, S., & Stutz, J. J. J. o. G. R. A. (2007). Intercomparison of multi-axis and long-path differential optical absorption spectroscopy measurements in the marine boundary layer. *112*(D10).
Pollack, I. B., Lerner, B. M., & Ryerson, T. B. J. J. o. a. c. (2010). Evaluation of ultraviolet light-emitting diodes for detection of atmospheric NO 2 by photolysis-chemiluminescence. *65*(2-3), 111- 125.
Pope III, C. A., Dockery, D. W. J. J. o. t. a., & association, w. m. (2006). Health effects of fine particulate air pollution: lines that connect. *56*(6), 709-742.
Pope III, C. A., Ezzati, M., & Dockery, D. W. J. N. E. J. o. M. (2009). Fine-particulate air pollution and life expectancy in the United States. *360*(4), 376-386.
Premuda, M., Petritoli, A., Masieri, S., Palazzi, E., Kostadinov, I., Bortoli, D., … Giovanelli, G. J. A. e. (2013). A study of O3 and NO2 vertical structure in a coastal wooded zone near a metropolitan area, by means of DOAS measurements. *71*, 104-114.
Riess, J. J. U. E. P. A., Office of Air Quality Planning, & Standards. (1998). Nox: how nitrogen oxides affect the way we live and breathe. 2.
Robinson, J. K., Bollinger, M. J., & Birks, J. W. J. A. c. (1999). Luminol/H2O2 chemiluminescence detector for the analysis of nitric oxide in exhaled breath. *71*(22), 5131-5136.
Roble, R. G. J. T. U. M., Experiment, L. T. A. R. o., & Theory, G. M. S. (1995). Energetics of the mesosphere and thermosphere. *87*, 1-21.
Rothman, L. S. J. J. o. Q. S., & Transfer, R. (2010). The evolution and impact of the HITRAN molecular spectroscopic database. *111*(11), 1565-1567.

Salonen, H., Salthammer, T., & Morawska, L. J. E. i. (2019). Human exposure to NO2 in school and office indoor environments. *130*, 104887.

Seaton, A., Godden, D., MacNee, W., & Donaldson, K. J. T. l. (1995). Particulate air pollution and acute health effects. *345*(8943), 176-178.

Serdyuchenko, A., Gorshelev, V., Weber, M., Chehade, W., & Burrows, J. J. A. M. T. (2014). High spectral resolution ozone absorption cross-sections–Part 2: Temperature dependence. *7*(2), 625-636.

Shabbir, Y., Khokhar, M. F., Shaiganfar, R., & Wagner, T. J. J. o. E. S. (2016). Spatial variance and assessment of nitrogen dioxide pollution in major cities of Pakistan along N5-Highway. *43*, 4- 14.

Shaiganfar, R., Beirle, S., Petetin, H., Zhang, Q., Beekmann, M., & Wagner, T. J. A. M. T. (2015). New concepts for the comparison of tropospheric NO 2 column densities derived from car-MAX-DOAS observations, OMI satellite observations and the regional model CHIMERE during two MEGAPOLI campaigns in Paris 2009/10. *8*(7), 2827-2852.

Takashima, H., Irie, H., Kanaya, Y., & Akimoto, H. J. A. e. (2011). Enhanced NO2 at Okinawa Island, Japan caused by rapid air-mass transport from China as observed by MAX-DOAS. *45*(15), 2593-2597.

Thalman, R., & Volkamer, R. J. P. c. c. p. (2013). Temperature dependent absorption cross-sections of O 2–O 2 collision pairs between 340 and 630 nm and at atmospherically relevant pressure. *15*(37), 15371-15381.

Theys, N., Roozendael, M. V., Hendrick, F., Fayt, C., Hermans, C., Baray, J.-L., . . . Physics. (2007). Retrieval of stratospheric and tropospheric BrO columns from multi-axis DOAS measurements at Reunion Island (21 S, 56 E). *7*(18), 4733-4749.

Tian, X., Xie, P., Xu, J., Li, A., Wang, Y., Qin, M., & Hu, Z. J. J. o. E. S. (2018). Long-term observations of tropospheric NO2, SO2 and HCHO by MAX-DOAS in Yangtze River Delta area, China. *71*, 207- 221.

Vandaele, A. C., Hermans, C., Simon, P. C., Van Roozendael, M., Guilmot, J. M., Carleer, M., & Colin, R. J. J. o. a. c. (1996). Fourier transform measurement of NO2 absorption cross-section in the visible range at room temperature. *25*(3), 289-305.

Vlemmix, T., Hendrick, F., Pinardi, G., Smedt, I. D., Fayt, C., Hermans, C., . . . Roozendael, M. V. J. A. M. T. (2015). MAX-DOAS observations of aerosols, formaldehyde and nitrogen dioxide in the Beijing area: comparison of two profile retrieval approaches. *8*(2), 941-963.

Vlemmix, T., Piters, A., Stammes, P., Wang, P., & Levelt, P. J. A. M. T. (2010). Retrieval of tropospheric NO 2 using the MAX-DOAS method combined with relative intensity measurements for aerosol correction. *3*(5), 1287-1305.

Wagner, T., Beirle, S., Brauers, T., Deutschmann, T., Frieß, U., Hak, C., … Li, X. J. A. M. T. (2011). Inversion of tropospheric profiles of aerosol extinction and HCHO and NO 2 mixing ratios from MAX-DOAS observations in Milano during the summer of 2003 and comparison with independent data sets. *4*(12), 2685-2715.

Wagner, T., Dix, B. v., Friedeburg, C. v., Frieß, U., Sanghavi, S., Sinreich, R., & Platt, U. J. J. o. G. R. A. (2004). MAX-DOAS O4 measurements: A new technique to derive information on atmospheric aerosols—Principles and information content. *109*(D22).

Wagner, T., Ibrahim, O., Shaiganfar, R., & Platt, U. J. A. m. t. (2010). Mobile MAX-DOAS observations of tropospheric trace gases. *3*(1), 129-140.

Wang, S., Zhou, B., Wang, Z., Yang, S., Hao, N., Valks, P., … Chen, L. J. J. o. G. R. A. (2012). Remote sensing of NO2 emission from the central urban area of Shanghai (China) using the mobile DOAS technique. *117*(D13).

Wang, Y., Lampel, J., Xie, P., Beirle, S., Li, A., Wu, D., & Wagner, T. (2017). Ground-based MAX-DOAS observations of tropospheric aerosols, NO2, SO2 and HCHO in Wuxi, China, from 2011 to

2014.

Wittrock, F., Oetjen, H., Richter, A., Fietkau, S., Medeke, T., Rozanov, A., . . . Physics. (2004). MAX-DOAS measurements of atmospheric trace gases in Ny-Ålesund-Radiative transfer studies and their application. *4*(4), 955-966.

Zafar, L., Ahmad, S., Syed, W., & Ali, S. J. S. I. (2012). Temporal variations in nitrogen dioxide concentration due to vehicular emissions in Islamabad capital territory (ICT) & Rawalpindi. *24*(3), 265-268.

Zhang, Q., Shen, Z., Cao, J., Zhang, R., Zhang, L., Huang, R.-J., . . . Xu, H. J. A. e. (2015). Variations in PM2. 5, TSP, BC, and trace gases (NO2, SO2, and O3) between haze and non-haze episodes in winter over Xi'an, China. *112*, 64-71.

CRAWFORD, J., PIERCE, G., LONG, R., SZYKMAN, J., LEITCH, J., NOWLAN, C., HERMAN, J., WEINHEIMER, A. & AL-SAADI, J. J. E. M. 2016. Multi-perspective observations of NO2 over the Denver area during DISCOVER-AQ: Insights for future monitoring. 66**,** 25-29.

HENDRICK, F., POMMEREAU, J.-P., GOUTAIL, F., EVANS, R., IONOV, D., PAZMINO, A., KYRÖ, E., HELD, G., ERIKSEN, P., DOROKHOV, V. J. A. C. & PHYSICS 2011. NDACC/SAOZ UV-visible total ozone measurements: improved retrieval and comparison with correlative ground-based and satellite observations. 11**,** 5975-5995.

Zhang, Y., Wang, Y., Chen, G., Smeltzer, C., Crawford, J., Olson, J., ... & Diskin, G. (2016). Large vertical gradient of reactive nitrogen oxides in the boundary layer: Modeling analysis of DISCOVER-AQ 2011 observations. *Journal of Geophysical Research: Atmospheres*, *121*(4), 1922-1934.